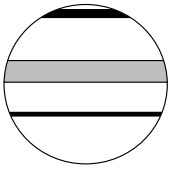

Research paper

The Holocene
2018, Vol. 28(9) 1411–1430

DOI: 10.1177/0959683618777070
journals.sagepub.com/home/hol
SAGE

Holocene sea-level change and coastal landscape evolution in the southern Gulf of Carpentaria, Australia

Craig R Sloss,[1] Luke Nothdurft,[1] Quan Hua,[2] Shoshannah G O'Connor,[1] Patrick T Moss,[3] Daniel Rosendahl,[4] Lynda M Petherick,[5] Rachel A Nanson,[6] Lydia L Mackenzie,[7] Alison Sternes,[1] Geraldine E Jacobsen[2] and Sean Ulm[4,8]

Abstract

A revised Holocene sea-level history for the southern Gulf of Carpentaria is presented based on new data from the South Wellesley Archipelago and age recalibration of previous research. Results confirm that rising sea levels during the most recent post-glacial marine transgression breached the Arafura Sill ca. 11,700 cal. yr BP. Sea levels continued to rise to ca. –30 m by 10,000 cal. yr BP, leading to full marine conditions. By 7700 cal. yr BP, sea-level reached present mean sea-level (PMSL) and continued to rise to an elevation of between 1.5 m and 2 m above PMSL. Sea level remained ca. + 1.5 between 7000 and 4000 cal. yr BP, followed by rapid regression to within ± 0.5 m of PMSL by ca. 3500 cal. yr BP. When placed into a wider regional context results from this study show that coastal landscape evolution in the tropical north of Australia was not only dependent on sea-level change but also show a direct correlation with Holocene climate variability. Specifically, the formation and preservation of beach-rock deposits, intertidal successions, beach and chenier ridge systems hold valuable sea-level and Holocene climate proxies that can contribute to the growing research into lower latitude Holocene sea-level and climate histories.

Keywords

Australia, beach ridge, beach-rock, chenier, coastal, Holocene, sea-level

Received 9 January 2018; revised manuscript accepted 28 March 2018

Introduction

The study of Holocene sea-level histories and coastal landscape response is fundamental to our understanding of how coastal environments will respond to future sea-level and climate change (McGowan and Baker, 2014; Williams et al., 2018). The Gulf of Carpentaria is an ideal locality for investigating changes in sea-level over the last glacial cycle. Positioned in a relatively tectonically stable portion of the Indo-Australian Plate, the southern Gulf of Carpentaria is positioned in a far-field region, unaffected by glacio-isostasy (Lewis et al., 2013). Located between Australia and New Guinea, the Gulf of Carpentaria is an epicontinental sea extending from 10ºS to 18ºS, and covering an area of around 230,000 km^2 (Figure 1a). At present, the Gulf of Carpentaria is connected to the Coral Sea in the northeast by the Torres Strait with water depths of up to 12 m. To the northwest, the Gulf is connected to the Arafura Sea through the Arafura Sill, with water depths of up to 53 m (Figure 1a; Chivas et al., 2001; Reeves et al., 2008). The seafloor in the Gulf is a relatively flat, featureless plain between 50 and 60 m water depth, with the greatest water depth of 70 m in the central eastern basin (Torgersen et al., 1983, 1988). The shallowness of the receiving basin, and restriction from marine influences during sea-level lowstands, provide an ideal location to investigate major phases of marine transgression and regression, recording fully marine, estuarine and lacustrine depositional environments for the past 200,000 years (Chivas et al., 2001; Reeves et al., 2007, 2008, 2013; Torgersen et al., 1983, 1988)

Previous research into sea-level change following the Last Glacial Maximum (LGM) in the Gulf of Carpentaria indicated that rising sea levels during the most recent post-glacial marine transgression (PMT) breached the restricting Arafura Sill between

[1]School of Earth, Environmental and Biological Sciences, Queensland University of Technology, Australia
[2]Australian Nuclear Science and Technology Organisation, Australia
[3]School of Earth and Environmental Sciences, The University of Queensland, Australia
[4]College of Arts, Society and Education, James Cook University, Australia
[5]School of Geography, Environment and Earth Sciences, Victoria University of Wellington, New Zealand
[6]Australian School of Petroleum, University of Adelaide, Australia. Current address: Environmental Geoscience Division, Geoscience Australia, Australia
[7]State Key Laboratory of Lake Science and Environment, Nanjing Institute of Geography and Limnology, Chinese Academy of Sciences, China
[8]ARC Centre of Excellence for Australian Biodiversity and Heritage, James Cook University, Australia

Corresponding author:
Craig R Sloss, School of Earth, Environmental and Biological Sciences, Queensland University of Technology, GPO Box 2434, Brisbane, QLD 4001, Australia.
Email: c.sloss@qut.edu.au

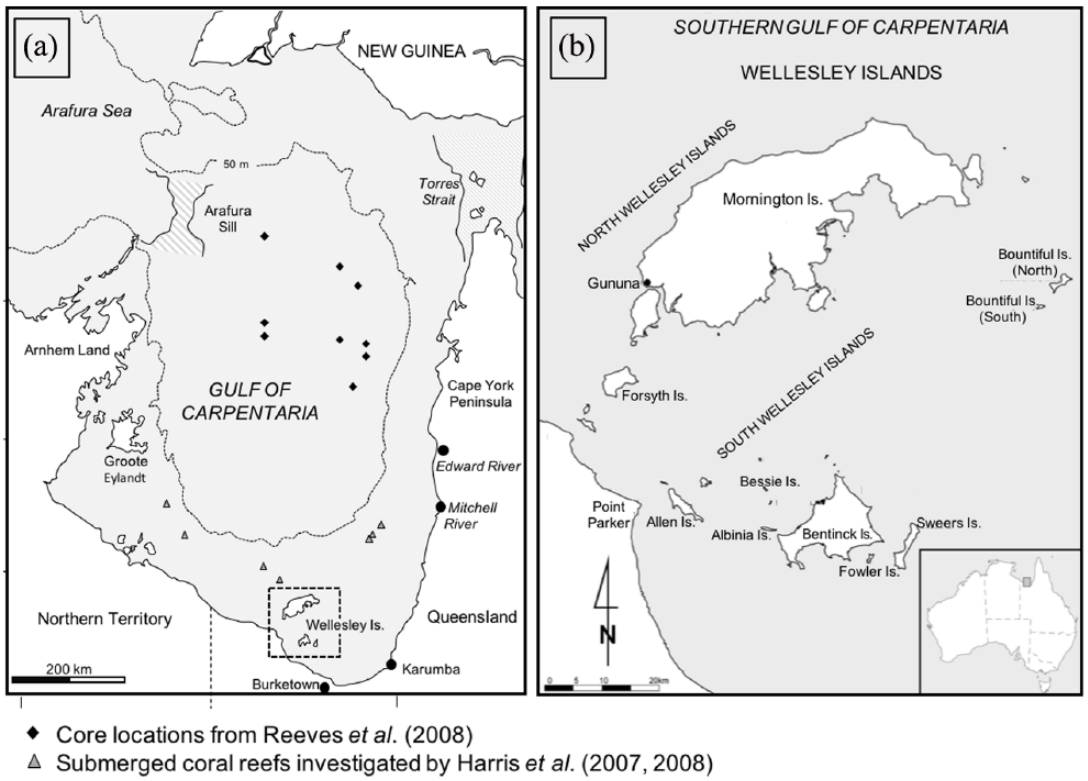

Figure 1. Location of (a) the Gulf of Carpentaria, northern Australia and (b) Wellesley Islands including the study sites, Bentinck, Sweers, Albinia and Fowler Islands.

12,000 and 11,500 cal. yr BP. The culmination of PMT occurred between 6500 and 6000 cal. yr BP, reaching a maximum of 2 m above present mean sea-level (PMSL) and then fell to present levels over the last 6000 years (Chappell et al., 1982; Rhodes et al., 1980). Rhodes et al. (1980) and Chappell et al. (1982) attribute the relative sea-level fall to hydro-isostatic loading in the northern and central basin, and on the eastern Australian continental shelf. Hydro-isostatic loading is argued to have caused differential crustal movement across north Queensland, represented by regional subsidence in the northeast and uplift of between 0.2 and 1.4 m for the western Cape York (Edward River), and 1.7 and 3.1 m in the Flinders-Leichhardt region (Karumba; Figure 1a; Chappell et al., 1982).

This study presents a revised Holocene sea-level history based on a review of previous research from the southern Gulf of Carpentaria and additional data collected from beach-rock and aeolianite deposits, cores from beach ridges, mudflats and mangrove swamps, survey of wave-cut erosional features, and dating of *in situ* encrusting organisms. The resulting detailed Holocene sea-level reconstruction is compared to other Holocene sea-level histories identified along the east coast of Australia (Lewis et al., 2013; Sloss et al., 2005, 2007; Woodroffe et al., 2007). Trends between sea-level histories over larger regional scales spanning across eastern Australia to the Gulf of Carpentaria are assessed, and drivers investigated to decipher if changes documented in the South Wellesley Archipelago is a result of localized hydro-isostatic influences or regional eustatic driving forces.

Study site: Wellesley Archipelago and adjacent mainland coast

The Wellesley Archipelago is a group of 23 islands in the southern Gulf of Carpentaria. Mornington (the northernmost and largest island at ca. 950 km^2) and Bentinck Island (ca. 150 km^2) comprise the traditional country of Lardil and Kaiadilt people, respectively. The remainder of the archipelago comprises smaller islands including Sweers, Fowler, Albinia, Horseshoe, Forsyth and Allen Islands (Figure 1b).

Located between the latitudes of 16°17'S and 17°09'S and longitudes of 139°02'E and 139°54'E, the Wellesley Islands have a tropical climate with a hot, wet summer monsoonal season and a warm, dry winter season. Summer air temperatures range from 28 to 35°C and winter air temperatures range from 22 to 30°C. Ninety-two percent of the average 1200 mm rainfall occurs from November to March, associated with the Australian Monsoon and cyclones (Bureau of Meteorology (BOM), 2016). Within the southern Gulf of Carpentaria, the neap tidal range averages 3 m, and reaches up to 4 m during spring tides (Church and Forbes, 1981; Rhodes et al., 1980; Wolanski, 1993).

The core of the islands is composed of Jurassic to Early Cretaceous fluvial and marine sedimentary successions comprising alternating sandstones, clayey sandstones and siltstones (the Normanton Formation) (Day, 1983; Grimes, 1979; Smart et al., 1980). The Normanton Formation is heavily weathered to a sandy lateritic surface with little relief, often forming wave-cut cliffs and platforms in coastal outcrop. The islands presently preserve a diverse range of Holocene coastal environments, including beach ridge systems, mangrove fringe and intertidal mudflats (ITM) and sandflats, and significant exposures of aeolianite. The adjacent coastal mainland sites include broad chenier plains and beach ridge deposits, first described by Rhodes et al. (1980) and Rhodes (1982). At some locations, shore parallel chenier ridge systems have prograded over 30 km since the mid-Holocene between Karumba and Burketown (Rhodes, 1982; Figure 1a).

Background

Over the late Quaternary, the Gulf has been repeatedly submerged and exposed by fluctuating sea levels with depositional environments shifting between open ocean to estuarine, lacustrine and subaerial exposure (Chivas et al., 2001; Reeves et al., 2008). Using micro-palaeontological indicators and radiocarbon age

determinations Yokoyama et al. (2000, 2001a, 2001b) identified that sea-level was 120 m below PMSL during the LGM. During this time, the Arafura and Torres Strait sills isolated the Gulf of Carpentaria from marine inundation, resulting in an extensive basin occupied by a large lake (Lake Carpentaria) up to 250 km in width, 500 km in length, and an average of 15 m deep (Jones and Torgersen, 1988; Reeves et al., 2008; Torgersen et al., 1988; Yokoyama et al., 2001a, 2001b).

Detailed palaeo-ecological and sedimentary analysis of lacustrine and marine basin sediments by Chivas et al. (2001) and Reeves et al. (2008) indicated that rising sea levels during the most recent PMT breached the Arafura Sill ca. 12,000 cal. yr BP, with full marine conditions being attained by 10,500 cal. yr BP. U-series dating of drowned coral reefs in the southern Gulf of Carpentaria indicate that reef growth commenced between 10,500 and 9500 cal. yr BP and continued to flourish until ca. 7000 cal. yr BP (Harris et al., 2007, 2008; Figure 1a).

The principal records for the timing and elevation of the culmination of most recent PMT sea-levels in the southern Gulf of Carpentaria derive from chenier ridges and beach ridge systems at Karumba and Edward River (Chappell et al., 1982; Rhodes, 1982; Rhodes et al., 1980; Figure 1). Previous research utilizing radiocarbon age determinations on the intertidal *Tegillarca granosa* (syn. *Anadara granosa*) sampled from chenier and beach ridge deposits suggested that sea-level was higher (ca. + 2.2 m) ca. 6000–5500 cal. yr BP, before falling to its present level (original ^{14}C ages in Chappell et al., 1982; Rhodes, 1982; Rhodes et al., 1980 calibrated for this study, see Table 4). This record of higher sea-level in the mid-Holocene provided one of the key datasets for modelling of hydro-isostatic adjustment in northern Australia (Chappell et al., 1982, 1983).

Sea-level proxies

To determine the indicative meaning (IM) of a sea-level 'index point', it is critical to establish the accuracy and precision of the elevation of the index point in relation to PMSL (Engelhart et al., 2009; Rovere et al., 2016; Shennan and Horton, 2002). In this section, we review the various sea-level index points used in previous research and in this study. Proxies include chenier and beach ridge systems, aeolianite deposits, *in situ* oyster beds and bioherms, intertidal and subtidal sedimentary successions, and erosional features. A critical assessment of the IM of the various proxies in relation to their contemporary sea-level at the time of deposition and/or formation, stratigraphic context, post-deposition alteration, and their position relative to PMSL (Australian Height Datum (AHD), equivalent to PMSL) are assessed (Lewis et al., 2013; Sloss et al., 2007; Woodroffe and Chappell, 1993). This incorporates establishing the indicative range (IR; the vertical range associated with the index point) and the reference water level (RWL; mid-point of the IR) in relation to PMSL (Engelhart et al., 2009; Rovere et al., 2016; Shennan and Horton, 2002). The IM is established using the formulas modified after Rovere et al. (2016)

$$RWL = \frac{U1 + L1}{2} \quad (1)$$

$$IM = E - RWL \quad (2)$$

$$IM_e = \sqrt{E_e^2 + \left(\frac{IR}{2}\right)^2} \quad (3)$$

where $U1$ is the upper limit of modern analogue, $L1$ is the lower limit of modern analogue, *RWL* is the mid-point of modern analogue (PMSL), *IR* is the indicative range of sea-level index point, and *E* is the elevation of sea-level index point, E_e is the elevation error associated with field measurement of index point, *IM* is the indicative meaning of sea-level index point, and IM_e is the vertical error associated with the IM of sea-level index point.

The modern analogue range in this study is taken from the maximum spring tide range (4 m) or in some specific cases the maximum neap tide range (3 m) observed in the Gulf of Carpentaria. The IM of the index points are expressed as elevations relative to PMSL (AHD).

Chenier ridge systems

Chenier ridges are wave-built landforms, deposited within the high-tide to supra-tidal zone and comprising two or more parallel to sub-parallel stranded ridges (cheniers) of coarse sediment (sand, gravel or shell). Such features are common on open coasts with low-to-moderate wave-energy environments with the coarse chenier ridges deposited over finer-grained intertidal deposits (Augustinus et al., 1989; McBride et al., 2007; Otvos, 2004, 2005; Weill et al., 2012). Formation occurs with the onshore migration of coarse sediment with rising tides and wave bores to the high-water spring tide (HWST) and mean high-water neap tide (HWNT) (McBride et al., 2007; Weill et al., 2012). As the ridge crest grows above the mean HWST, they become less frequently submerged and are starved of sediment (Weill et al., 2012). A chenier plain forms when two or more sets of chenier ridges are separated by fine-grained intertidal deposits and are characteristic of prograding coastlines (McBride et al., 2007; Otvos, 2004, 2005). The formation of chenier ridges and plains is also strongly influenced by episodic sediment supply (seasonal), as well as the influence of storms, sea-level fluctuations, longshore currents, tidal dynamics and delta development (Augustinus, 1989; Dougherty and Dickson, 2012; McBride et al., 2007; Nanson et al., 2013; Nott, 1996; Saito et al., 2001).

Despite the dynamic depositional processes, the transition between the chenier ridges and underlying intertidal muds can be used to reconstruct Holocene sea-level histories (e.g. Dougherty and Dickson, 2012; McBride et al., 2007; Rhodes, 1982; Rhodes et al., 1980; Saito et al., 2000; Wang and van Strydonck, 1997; Weill et al., 2012). For example, Dougherty and Dickson (2012) demonstrated that a clear stratigraphic boundary exists between chenier ridges and underlying intertidal mud facies using Ground Penetrating Radar (GPR) across the Miranda chenier plain on the North Island of New Zealand. Dougherty and Dickson (2012) identified the upper limit of this stratigraphic transition to be the equivalent of the HWST, and identified changes in sea level controlled chenier spacing.

Accordingly, chenier ridges provide a proxy for palaeo-sea-level (between HWNT to HWST), but cannot provide an upper limit, as they can be deposited above mean sea-level (Figure 2). Age determination from chenier ridges must also be used with caution as faunal components are transported and reworked, and any age determinations require careful assessment of the accuracy, precision and relevance of the chronological framework developed. In this study, an IM for chenier ridges as a sea-level proxy is taken from the facies transition from intertidal and subtidal mudflat deposits with the overlying chenier ridge representing an IR of 1.5–2 m above PMSL and an IM of + 1.75 m (Figure 2).

Beach ridge systems

Beach ridge deposits are parallel to sub-parallel elongate mounds of fine-grained sand to boulder size material, comprising of siliciclastic or bioclastic sediments. Beach ridges form from the interplay of nearshore processes (tides, currents and waves), sediment supply and physical characteristics (e.g. grain size and lithology), and are common features on prograding coasts with flat nearshore topography and abundant sediment supply (Brooke et al., 2008;

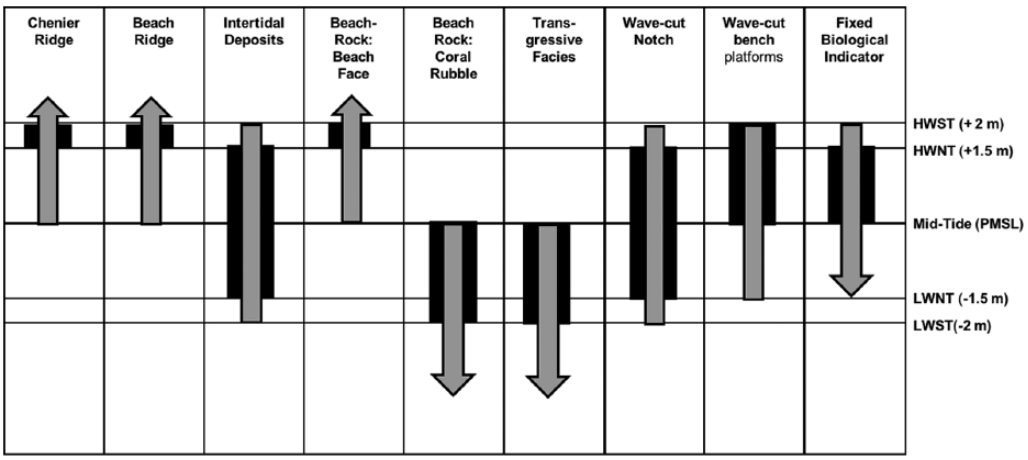

Figure 2. Schematic representation of sea-level index points relative to tidal range in the Gulf of Carpentaria, with a neap tide range of 3 m and spring tide range of 4 m. Transgressive facies within sedimentary successions discussed in results have been included. Grey arrow represents the maximum potential range of the observed proxy. The black box representing the refined indicative meaning based on facies associations.

Otvos, 2000; Scheffers et al., 2011; Tamur, 2012; Taylor and Stone, 1996). The established mode for sandy beach ridge formation involves the beach-face receiving sediment transported shoreward, resulting in progradation under fair-weather wave conditions (Komar, 1998; Otvos, 2000). As the coastline progrades, the beach ridges and inter-dune swales are stranded and preserve a palaeo-environmental record (Dougherty, 2014; Otvos, 2000; Tamur, 2012; Tanner, 1988; Taylor and Stone, 1996).

In contrast to chenier deposits, beach ridges are underlain by nearshore beach sediments and provide an opportunity to investigate palaeo-depositional environments and past sea-level highstands (Otvos, 2000, 2005; Rodriguez and Meyer, 2006; Tamur, 2012). However, sea-level studies based on ridge plain elevations and geometry are problematic due to ridges aggrading well above high tide, with significant variations in lateral elevation (Nott et al., 2013; Otvos, 2005). To use beach ridges as palaeo sea-level indicators, the boundary between the underlying beach-face and the overlying back-beach deposits, in addition to the overlying aeolian facies, needs to be correctly identified. The transition between the foreshore (low tide to high tide, and characterized by gentle seaward-dipping planar bedding) and backshore facies (characterized by gentle landward-dipping planar bedding) is formed at the level of landward swash limit of constructive waves, and is regarded as an indicator of the upper tidal level (Otvos, 2000, 2005). In the South Wellesley Islands, prograding beach ridge systems are a common feature on Bentinck Island and the adjacent mainland (Figures 3 and 4). In this study, an IM associated with beach ridges as a record of past sea-level is taken from the transition from the beach-face to back-beach deposits (between HWNT and HWST; (IR) = +1.5 to +2 m; (IM) = +1.75 m; Figure 2).

Intertidal and subtidal mangrove and mudflat deposits

Sedimentary successions preserved in ITM and intertidal sand flats (aka. salt/clay pans), and associated mangroves and mangrove sediments, have been used along the southeast coast of Australia as indicators of past sea-level (Beaman et al., 1994; Grindrod and Rhodes, 1984; Grindrod et al., 1999, 2002; Sloss et al., 2005, 2007, 2011; Lewis et al., 2013), as well as globally (Hendry and Digerfeldt, 1989; Parkinson, 1989; Scholl, 1964; Scholl et al., 1969; Woodroffe, 1981). Sedimentary deposits associated with intertidal and mangrove deposits are generally distributed between mid-tide and mean HWNT (Beaman et al., 1994; Grindrod and Rhodes, 1984; Lewis et al., 2013; Sloss et al., 2007, 2011). Accordingly, intertidal and mangrove deposits provide useful indicators of when sea-level attained a particular elevation. However, as with other proxies, intertidal depositional environments are less useful for maximum sea-level as they can be deposited between LWST and HWST. Issues relating to the stratigraphic reliability and precision of such deposits as sea-level indicators have been summarized in Sloss et al. (2007), Smithers (2011) and Lewis et al. (2013).

Within the South Wellesley Islands mudflats form extensive features isolated from the open ocean by the mangrove fringe (Figures 2 and 3). The mudflats investigated in this research are now preserved up to 2 m above PMSL and retain a record of coastal landscape evolution over the Holocene. For both mangrove deposits and ITMs, the IR is between LWNT and HWNT (IR = −1.5 – +1.5 m; *IM* = 0 m; Figure 2).

Beach-rock

Beach-rock comprises cemented beach sands and is usually found as clearly bedded outcrops of moderately-to-well consolidated sediment, preserving the internal structure of beach facies. The formation of beach-rock has been debated in the literature for several decades, although it is now recognized that it can form through several different processes (see McLean, 2011, and references therein). It is generally agreed that beach-rock forms in the intertidal zone when unconsolidated sediments become lithified by precipitation of aragonite and/or calcite cements, preserving the internal fabric of the beach stratigraphy. Outcrops can be over 3 m thick in areas with relatively high tidal ranges or exposed to high waves/swell conditions (Hopley, 1986; McLean, 2011). While beach-rock may provide a relatively constrained sea-level indicator in micro-tidal environments, the upper-most limit of formation is difficult to determine in areas with higher tidal ranges (Hopley, 1986; Hopley et al., 2007).

The use of beach-rock as a sea-level indicator is also problematic because it is difficult to determine a precise age for its formation. The constituent grains that formed the beach sand before lithification are almost certain to range across a wide temporal span. Accordingly, the dating of shell material in beach-rock provides an indicative age. Well-cemented beach-rock can also undergo several diagenetic phases (Vousdoukas et al., 2007). Consequently, the dating of cements can generate different ages to any biogenic carbonate, providing a minimum age (Desruelles et al., 2009).

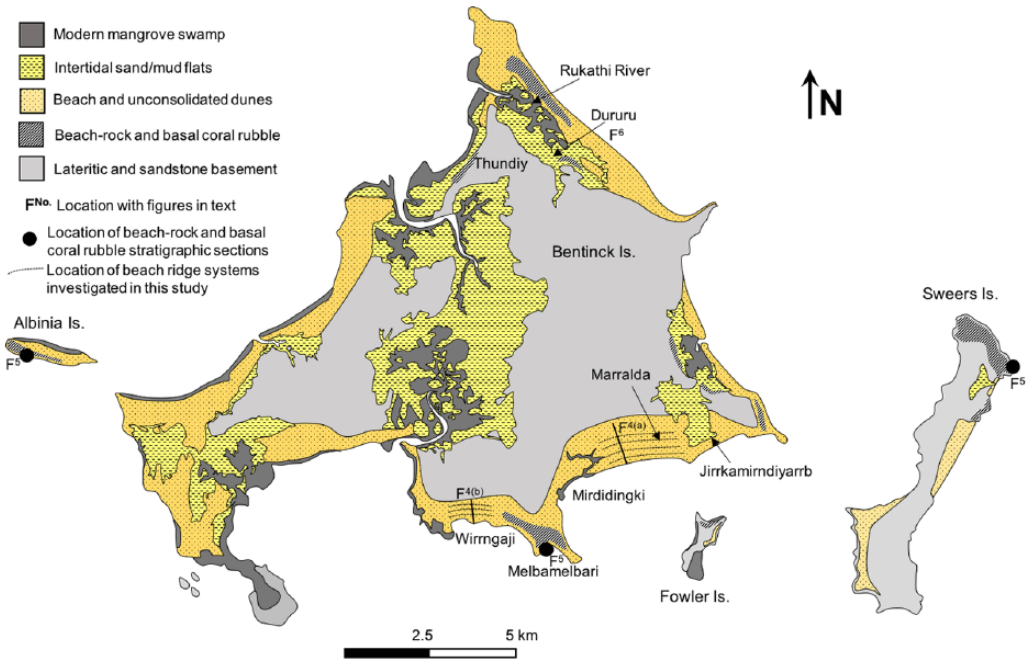

Figure 3. Location and facies map of Bentinck, Sweers, Fowler and Albinia Islands showing various geomorphological features and study sites.

Regardless of the issues associated with utilizing beach-rock as sea-level indicators, the facies association between beach-face and back-beach deposits can be used as an indicator of past sea-level (Hopley, 1986; Pirazzoli, 1996). For example, on continental islands in northeastern Australia, Hopley (1986) determined the vertical error range for beach-rock as a sea-level proxy as the maximum tidal range with an unknown upper level associated with HWST. A more precise sea-level proxy can be established by identifying the boundary between the intertidal beach facies and overlying back-beach and aeolian deposits, restricting the sea-level to the upper intertidal zone (Hearty et al., 2007; Hopley, 1986; Stattegger et al., 2013).

In the South Wellesley Islands, extensive partially-to-fully lithified beach-rock coastal outcrops up to 4 m above PMSL provide evidence for coastal deposition associated with the most recent PMT (Figures 2 and 3). The beach-rock deposits preserve sedimentary structures associated with nearshore (beach-face) and backshore facies, and thus provide a sea-level proxy. This transition is equivalent to the modern facies transitions in nearshore and beach successions (between HWNT and HWST; (IR) = +1.5 to +2 m; (*IM*) = +1.75 m; Figures 2, 3 and 5). Abundant mollusks associated with the nearshore facies association also provide material for constraining a maximum age for these deposits.

Intertidal erosional indicators

Erosional features that form in the intertidal zone such as wave-cut notches and wave-cut platforms have been used as indicators for past sea-levels in many parts of the world (e.g. Benac et al., 2004; Hearty et al., 2007; Kershaw and Guo, 2001; Pirazzoli, 1996; Rovere et al., 2016; Smithers, 2011). These intertidal erosional features are typically carved into softer rocks such as limestones, and form from a combination of physical weathering (wave action in the intertidal zone), chemical weathering during subaerial exposure during low tide, and biological abrasion (Hearty et al., 2007; Kershaw and Guo, 2001; Pirazzoli, 1996). Wave-cut platforms and notches form around mean sea-level in the intertidal zone and can form over tens to a few hundred years, and thus record previous prolonged sea-level highstands (Brooke et al., 2017; Hearty et al., 2007; Neumann and Hearty, 1996; Pirazzoli, 1986).

Although notches provide geomorphological evidence of former sea-level positions, they can rarely be dated accurately, and can only provide a relative age assessment. In the South Wellesley Islands, elevated wave-cut benches and notches are common geomorphological features on exposed rocky coasts (Figures 3, 5 and 6). The wave-cut features have been eroded into the Normanton Formation comprising easily eroded weathered lateritic sandstones and siltstones, or into moderately consolidated beach-rock, and are overlain by late Holocene beach ridges and aeolian deposits. Modern examples of wave-cut notches occur between LWNT and HWNT (IR = −1.5 – +1.5 m; *IM* = 0 m), and wave-cut benches/platforms between mid-tide and HWST (IR = 0 – +2 m, *IM* = + 1 m; Figures 2 and 3).

Encrusting organisms and oyster bioherm

Encrusting organisms, such as oysters, tubeworms and barnacles (Fixed Biological Indicators; FBIs), are confined to a restricted range within the intertidal zone on rocky shorelines, and have been utilized as sea-level indicators. For example, relict oyster beds, barnacle and tubeworm deposits have been used to constrain the elevation and duration of the mid-Holocene highstand along the east and west coasts of Australia (Beaman et al., 1994; Baker and Haworth, 1997, 2000a, 2000b; Baker et al., 2001a, 2001b, 2005; Lewis et al., 2008, 2015). A detailed review of the use of FBIs as proxies for sea-level reconstructions is provided in Sloss et al. (2007) and Lewis et al. (2008, 2013, 2015)

In the Wellesley Islands, the encrusting oyster *Striostrea (Parastriostrea) mytiloides* (common name black-lipped/black-edged oyster), commonly occur on elevated beach-rock deposits, wave-cut benches, and as mono-specific bioherm accumulations on exposed mudflats (Rosendahl et al., 2015). *S. mytiloides* is an intertidal species that commonly inhabits water levels from mid-tide to upper-tidal limits (HWNT) attached to rocks and mangrove roots. Therefore, the presence of encrusted *S. mytiloides* on elevated coastal landforms, and the growth of bioherm accumulations provide a sea-level index point from mid-tide to a maximum of HWNT (IR = 0 – 1.5 m, IM = + 0.75 m; Figures 2, 3 and 6).

Table 1. Location and details of auger, pit and stratigraphic sections from the South Wellesley Islands (note that multiple cores were taken at some locations).

Environment	Location	Core code/log code	Latitude (South)	Longitude (East)	Core AHD (m)	Core depth (cm)
Intertidal mud-flats	Thundiy	THU-01	17° 0' 15.9000"	139° 29' 41.5800"	1.60	1.40
		THU-02	17° 0' 48.6000"	139° 29' 40.1400"	1.70	0.80
		THU-03	17° 1' 04.3800"	139° 29' 32.1000"	1.50	0.20
		THU-04	17° 1' 38.2800"	139° 29' 03.7800"	1.60	2.90
		THU-05	17° 1' 46.1400"	139° 28' 43.2600"	1.65	2.20
		THU-06	17° 1' 50.2200"	139° 28' 50.6400"	1.60	3.80
		THU-07	17° 1' 53.1000"	139° 28' 57.4800"	1.60	1.40
		THU-08	17° 1' 54.0600"	139° 27' 27.3600"	1.65	1.55
		THU-09	17° 1' 25.6200"	139° 29' 13.9800"	1.65	2.70
		THU-10	17° 1' 54.4200"	139° 29' 13.9800"	1.60	2.30
		THU-11	17° 1' 54.4200"	139° 29' 13.9800"	1.60	1.45
		THU-12	17° 1' 11.8800"	139° 29' 54.2400"	1.70	1.80
		THU-13	17° 0' 53.5200"	139° 29' 24.4800"	1.75	1.30
		THU-14	17° 1' 52.1400"	139° 29' 37.9800"	1.80	1.50
	Dururu	DUR-01	17° 1' 18.9313"	139° 31' 01.0312"	2.54	2.10
		DUR-02	17° 1' 18.7662"	139° 30' 59.5375"	2.36	1.70
		DUR-03	17° 1' 15.4739"	139° 30' 57.3336"	1.92	0.40
		DUR-04	17° 1' 17.5051"	139° 30' 59.3162"	2.25	1.90
		DUR-05	17° 1' 19.5595"	139° 31' 01.7808"	2.59	6.00
Beach-ridge system	Marralda Wirrngaji	MIR-01	17° 5' 49.6320"	139° 32' 50.8920"	4.90	1.00
		MIR-02	17° 5' 44.0400"	139° 32' 45.9000"	4.20	3.20
		MIR-03	17° 5' 41.9400"	139° 32' 45.9000"	5.80	1.35
		MIR-04	17° 5' 37.4400"	139° 32' 45.6600"	4.20	2.10
		MIR-05	17° 5' 39.3000"	139° 32' 45.6000"	5.15	1.30
		MIR-06	17° 5' 35.7000"	139° 32' 32.6000"	4.45	0.75
		MIR-07	17° 5' 33.1200"	139° 32' 45.2400"	5.30	2.70
		MIR-08	17° 5' 27.8400"	139° 32' 43.9200"	5.75	0.50
		MIR-09	17° 5' 25.3200"	139° 32' 43.9200"	5.85	1.60
		MIR-10	17° 5' 51.2400"	139° 32' 43.9200"	3.80	2.50
		MIR-11	17° 5' 43.3800"	139° 32' 53.7200"	3.30	1.90
		MIR-12	17° 5' 26.2200"	139° 32' 43.8000"	6.50	4.00
		MIR-13	17° 5' 23.9400"	139° 32' 43.8600"	3.50	1.50
		MIR-14	17° 5' 51.6120"	139° 27' 23.0400"	4.25	1.10
		WIR-02	17° 6' 48.0000"	139° 29' 10.2000"	4.15	1.00
		WIR-03	17° 6' 51.0600"	139° 29' 13.2000"	4.10	0.80
		WIR-04	17° 6' 52.7400"	139° 29' 15.4800"	4.25	1.40
		WIR-05	17° 6' 55.6400"	139° 29' 17.5200"	3.70	2.40
Beach-rock	Bentinck Is. South	BS1-1A	17° 6' 53.9800"	139° 29' 40.0000"	Stratigraphic	
	Sweers Is. North	SE11	17° 6' 53.9800"	139° 38' 21.8800"	Stratigraphic	
	Albinia Is.	Alb1	17° 1' 19.5400"	139° 12' 45.1600"	Stratigraphic	
Elevated wave-cut bench/notch	Bentinck Is.	N/A	17° 1' 41.5600"	139° 31' 40.8200"	Profile	
	Fowler Is.	N/A	17° 7' 06.3900"	139° 33' 33.2400"	Profile	
	Albinia Is.	N/A	17° 1' 19.5400"	139° 12' 45.1600"	Profile	

Methods

Field based data: Beach ridges, intertidal and subtidal mudflats, beach-rock and fixed biological indicators

Augering, D-Section coring, trenches and pits were undertaken to construct stratigraphic sections for beach ridge systems (n = 18), ITMs and mangrove swamps (n = 19) and from coastal beach-rock exposures on Bentinck, Sweers and Albinia Islands (n = 3; Table 1; Figure 2). Individual facies based on field observations of sedimentary characteristics (grain size, sorting, roundness, lithology), observed sedimentary structures, and faunal elements (Table 1; Figures 3–6) were used to establish facies associations and depositional environments. Mollusks were collected from stratigraphic sections to identify faunal assemblages, establish their taphonomic history where possible, and for radiocarbon age determination (Sloss et al., 2011). Intertidal erosional indicators comprising wave-cut benches and wave-cut notches on Sweers, Albinia and Fowler Islands were surveyed into PMSL. Encrusting *Striostrea (Parastriostrea) mytiloides* preserved on elevated wave-cut benches and preserved in beach-rock deposits were sampled for radiocarbon dating (Figure 3; Tables 1, 4 and 5). All stratigraphic sections and wave-cut features were surveyed into the AHD (official height datum for Australian which equates to mean sea-level; Geocentric Datum of Australia, 1998; Lewis et al., 2013; Sloss et al., 2007; Umitsu et al., 2001). Surveys were conducted using a Real Time Kinematic (RTK) Geographic Positioning Systems (GPS), with a vertical error of approximately 5 cm.

Geochronology

In total, there are 143 previously published radiocarbon (Tables 3 and 4), 15 uranium-thorium (U-Th; Table 2), and 4 thermoluminescence (TL) and optical-stimulated luminescence (OSL; Table 4) age determinations from the southern and central Gulf of Carpentaria, with an accurate description of facies association and stratigraphic relationship to PMSL (AHD) (Harris et al., 2008; Nanson et al., 2013; Reeves et al., 2008, 2013; Rhodes, 1982; Rhodes et al., 1980; Rosendahl et al., 2015).

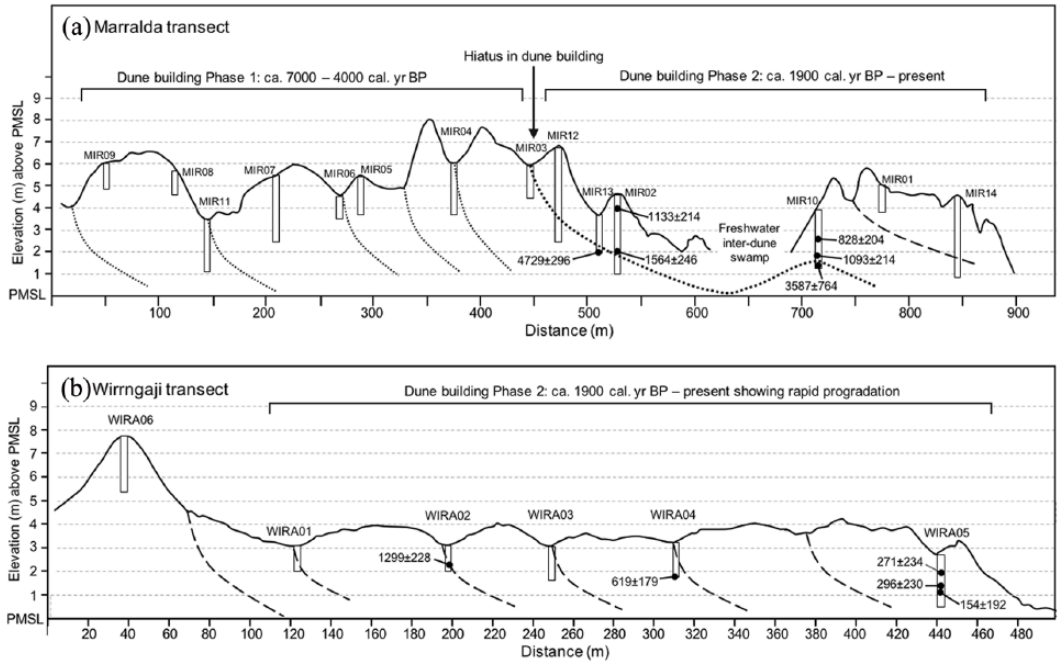

Figure 4. Profiles from Marralda and Wirrngaji and representative composite stratigraphic section of coastal beach ridge systems.

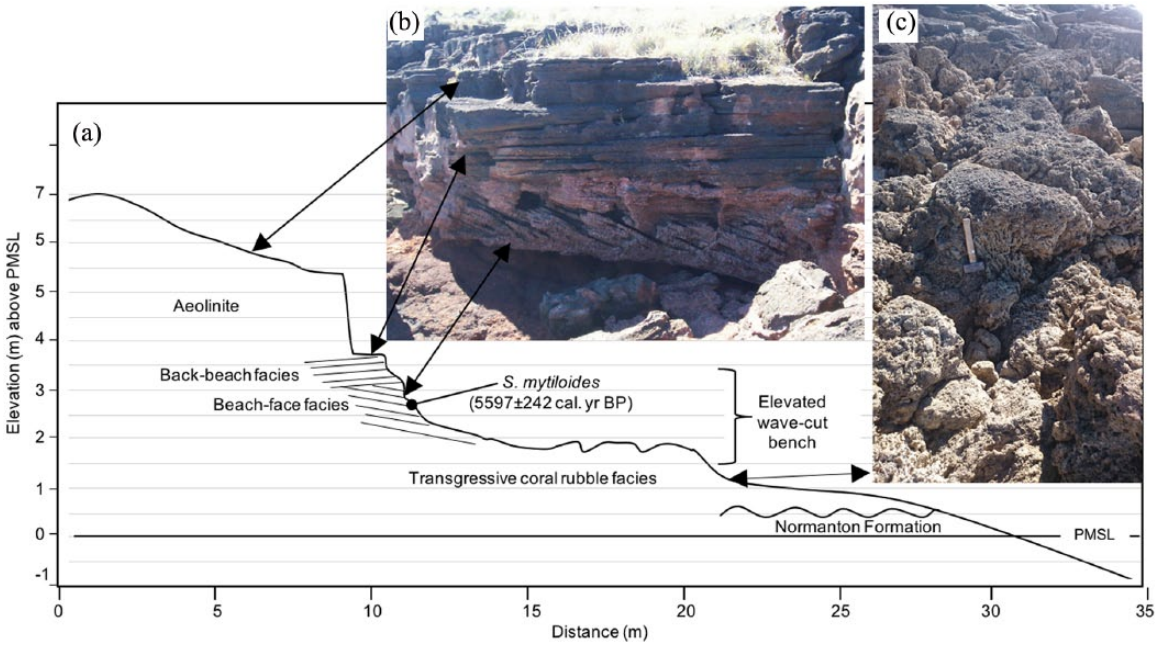

Figure 5. Representative profile and composite stratigraphic section of beach-rock outcrop identified on Bentinck, Sweers and Albinia Islands. (a) Profile of wave cut bench into beach-rock deposits on Albinia Island, (b) example of transition between seaward dipping (beach-face) and landward dipping (back-beach) planar bedding preserved in beach rock-deposits on Albinia Island, and, (c) example of *in situ* and reworked coral rubble associated with the most recent PMT on Sweers Island.

Additional 36 AMS radiocarbon age determinations were obtained from the Australian Nuclear Science and Technology Organization (ANSTO; Fink et al., 2004; Hua et al., 2001) and University of Waikato Radiocarbon Dating Laboratory, New Zealand (Table 5). Radiocarbon age determinations were obtained on samples of fossil marine mollusks and terrestrial organic material. Age determinations were calibrated to sidereal years using the radiocarbon calibration programme OxCal v.4.2 (Bronk Ramsey, 2009). Calibration for marine fossil mollusks collected in this study and from previous research used the marine calibration curve Marine13 (Reimer et al., 2013) with a marine reservoir correction for the southern Gulf of Carpentaria ($\Delta R = -49 \pm 102$ yr; Memmott et al., 2016; Ulm, 2006; Ulm et al., 2010) to correct for the marine reservoir effect, and convert ages into sidereal years (expressed as cal. yr BP; Tables 2–5; Gillespie, 1977; Gillespie and Polach, 1979; Stuiver et al., 1998; Sloss et al., 2013; Table 2–5). Age calibration for terrestrial samples was performed using the IntCal13 calibration data (Reimer et al., 2013). IntCal13 was used due to the influence of Northern Hemisphere air masses on the Tropical North of Australia, when the Inter Tropical Convergence Zone moves southwards during the Australian-Indonesian summer monsoons (Hogg et al., 2013; Hua et al., 2012).

Four uranium-series age determinations were undertaken on two coral samples from Sweers Island (Table 5). These samples were selected due to their high percentage of aragonite (>95%)

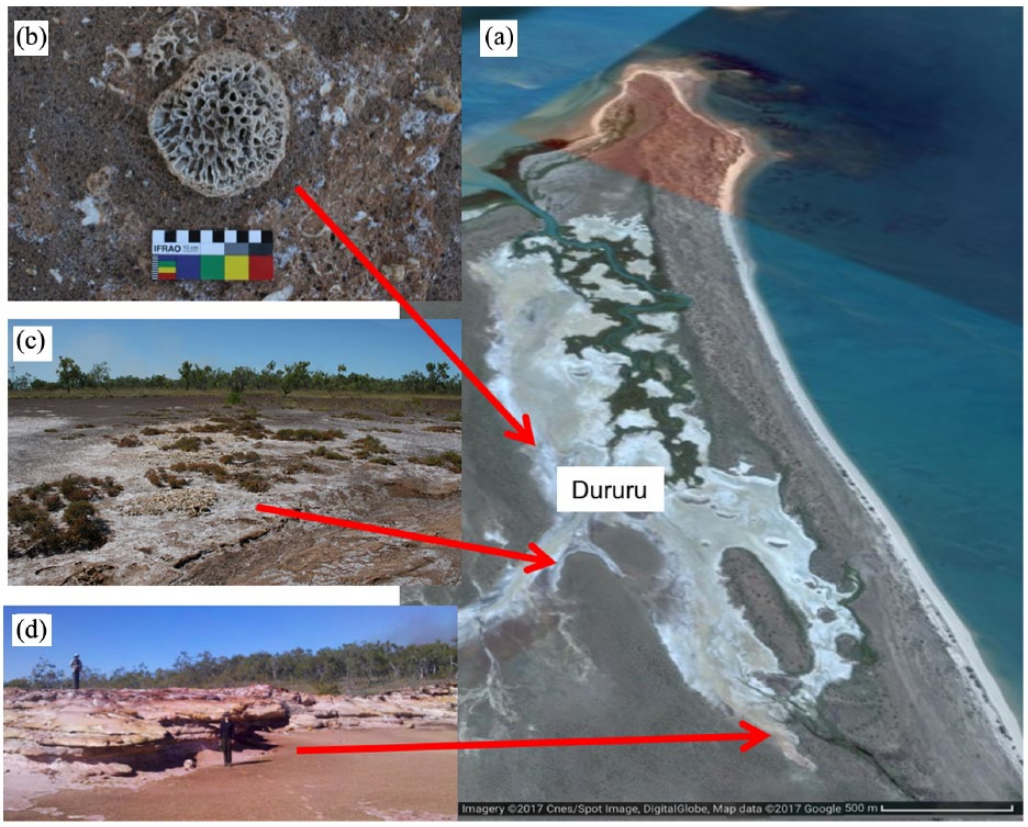

Figure 6. Representative profile of intertidal successions at Rukathi River and location of examples of various sea-level proxies utilized in this research. (a) Rukathi River supratidal mudflats, (b) *in situ* coral head preserved in partially consolidated beach-rock deposits at Dururu, (c) elevated accumulation of *in situ S. mytiloides* overlying partially consolidated beach-rock deposits at Dururu, and (d) wave-cut notch into Normanton Formation.

indicating an almost 'closed' system, where minimal diagenesis has occurred. U-Th dates were acquired with multi-collector inductively coupled plasma mass spectrometry (MC-ICP-MS) at the Radiogenic Isotope Facility (RIF), The University of Queensland, using the methods of Leonard et al. (2013), Zhou et al. (2011) and Clark et al. (2012).

All calibrated ^{14}C ages from the previous research and this study are reported at the 2σ age range, median and mean ± 2σ in cal. yr BP. All TL and OSL ages from the previous research and U-Th ages from this study are also reported as cal. yr BP. To be compatible with the TL, OSL and U-Th ages, which are shown in mean ages ± 2σ, all calibrated radiocarbon ages are also discussed in the text as mean ages ± 2σ.

Results

Geochronology

Radiocarbon ages (n = 36) were obtained from ITM and estuarine successions, beach ridge systems, elevated beach-rock and FBIs. Uranium-series dates (n = 4) were obtained on two fossil corals (Figure 3, Table 5). Dating methods, sample location, material/species, laboratory codes, and age determinations are expressed as uncorrected and calibrated ages with their associated error margins (Table 5). Sample elevations, age determinations and associated facies as well as the stratigraphic relationship of specific facies have also been determined relative to PMSL.

Beach ridge systems (BRdg)

Transects of augers and trenches across a beach ridge system were undertaken at Marralda and Wirrngaji on Bentinck Island. The Marralda/Mirdidingki beach ridge system comprises 10 individual ridges and extends 900 m inland, with an elevation of 3 to 8 m and an average elevation of 5 m above PMSL. The Wirrngaji beach ridge system comprises 7 individual ridges and extends 500 m inland with elevations from 4 to 8.75 m, and an average elevation of 4.6 m above PMSL. Three main facies were identified common to both transects (Figures 3 and 4).

1. A basal unit comprising rounded, medium-to-coarse-grained, moderately sorted mixed siliciclastic and carbonate sand. Faunal elements include present to common disarticulated and rare articulated marine and estuarine bivalves dominated by *Marcia hiantina* and *Gafrarium pectinatum* and the gastropod *Telescopium telescopium* (Table 6). Abundant shell fragments, shell hash and rounded-to-well-rounded ironstone pisoliths are common. In trenched sections, low-angled seaward dipping planar beds were observed, often defined by interbedded densely-packed shell beds, shell hash and pisoliths. The facies is interpreted as a beach-face within the beach ridge system (BRdg/BF). A radiocarbon age determination from a reworked *M. hiantina* valve provides a potential maximum age for the facies of ca. 5000 cal. yr BP (Tables 5 and 6; Figure 4).
2. Overlying the basal unit is a fine- to medium-grained, moderately sorted siliciclastic quartz sand with a minor component of carbonate shell fragments. Sub-horizontal to very low angled landward dipping planer bedding was observed in trench and pits. Broken disarticulated valves including *M. hiantina, Mactra* sp. and *G. pectinatum* are weathered and abraded, shell fragments and shell hash are common. The facies is interpreted as a reworked back-beach deposit (BRdg/BB). Radiocarbon age determinations from reworked faunal elements indicate an age range of ca. 3500 to 300 cal. yr BP (Tables 5 and 6; Figure 4).

Table 2. U-Th Ages on submerged coral reefs (Harris et al., 2008).

Environment	Core code	Core water depth (m)	Sample interval	Sample Relative to PMSL (m)	U-Th age (cal. yr BP)
Southern Gulf: Submerged *in situ* corals. Harris et al. (2008).	RD01	−26.8	0.39–0.40	−26.8	9285 ± 77
	RD07	−26.4	0.53–0.54	−26.4	9608 ± 77
	RD08	−29.2	0.37–0.38	−29.2	9661 ± 105
	RD09	−24.4	0.28–0.29	−26.4	8947 ± 62
	RD12	−20.2	0.19–0.20	−20.2	8355 ± 42
	RD12	−20.2	0.90–0.91	−20.2	8506 ± 54
	RD12	−20.2	1.76–1.77	−20.2	9424 ± 53
	RD18	−25.6	0.31–0.32	−25.6	9831 ± 75
	RD27	−29.6	0.15–0.16	−29.6	6966 ± 190
	RD28	−29.2	0.44–0.45	−29.2	9529 ± 111
	RD30	−25.6	0.78–0.79	−25.6	9736 ± 13
	RD33	−25.2	0.61–0.62	−25.2	7905 ± 10
	RD35	−30.4	0.15–0.16	−30.4	7429 ± 16
	RD37	−24.8	0.53–0.54	−24.8	9505 ± 10
	RD39	−27.6	0.35–0.36	−29.2	9911 ± 40

Table 3. Previous published radiocarbon ages from the central Gulf of Carpentaria: molluscs recovered from cores in the central basin (cf. Figure 1a; Reeves et al., 2008).

Environment	Core code	Core water depth (m)	Sample core depth (m)	Sample relative to PMSL (m)	Lab. code	Conventional ^{14}C age (yr BP (1σ))	Calibrated ^{14}C age (cal. yr BP)	
							2σ age range (median)	Mean ± 2σ
Non-marine*	MD28	−62	0.6	−62.6	OZG374	10,260 ± 80	11,715–12,392 (12,017)	12,022 ± 362
	MD31	−59	0.75	−59.8	OZG222	10,320 ± 60	11,839–12,405 (12,150)	12,160 ± 278
	MD31	−59	0.65	−59.7	OZE251	10,350 ± 100	11,824–12,539 (12202)	12,194 ± 374
	MD32	−64	0.35	−64.4	OZF290	10,380 ± 70	11,997–12,527 (12,249)	12,248 ± 268
	MD30	−60	0.7	−60.7	OZE250	10,410 ± 80	12,022–12,552 (12,285)	12284 ± 290
	MD30	−60	0.8	−60.8	OZG231	10,430 ± 80	12,040–12,565 (12,311)	12,309 ± 292
	MD30	−60	0.9	−60.9	OZG382	10,680 ± 70	12445–12732 (12,639)	12,631 ± 116
	MD31	−59	1.4	−60.4	OZI054	10,990 ± 110	12,711–13,065 (12,876)	12,881 ± 200
	MD32	−64	0.4	−64.4	OZF291	11,440 ± 80	13,120–13,445 (13,282)	13,282 ± 170
	MD30	−60	1.5	−61.5	OZF286	11,807 ± 170	13,305–14,052 (13,651)	13,665 ± 382
	MD32	−64	0.7	−64.7	OZF292	12,390 ± 80	14,116–14,921 (14,473)	14,490 ± 428
	MD32	−64	1	−65	OZG385	14,907 ± 130	17827–18465 (18133)	18136 ± 320
	MD28	−62	0.75	−62.7	OZG375	14,280 ± 90	17,105–17,646 (17,391)	17,385 ± 280
	MD32	−64	1.45	−65.5	OZG388	14,330 ± 100	17,130–17,752 (17,458)	17,452 ± 306
	MD32	−64	1.2	−65.2	OZG386	14,330 ± 90	17,148–17,721 (17,459)	17,453 ± 282
	MD28	−62	0.67	−62.7	OZE254	14,350 ± 90	17,180–17,765 (17,486)	17,481 ± 284
	MD32	−64	0.75	−64.8	OZG378	14,390 ± 80	17,272–17,818 (17,539)	17,539 ± 258
	MD33	−68	0.77	−68.8	OZE253	14,550 ± 100	17472–17978 (17,727)	17,726 ± 260
	MD28	−62	0.7	−62.7	OZG373	14,960 ± 90	17936–18421 (18,183)	18182 ± 248
	MD32	−64	1.5	−65.5	OZF293	15,390 ± 110	18,412–18,877 (18,658)	18,652 ± 230
	MD33	−68	0.77	−68.8	OZE252	15,760 ± 90	18,803–19,254 (19,012)	19,023 ± 230
	MD32	−64	2.34	−66.3	OZI055	18,320 ± 170	21,792–22,518 (22,173)	22,163 ± 380
	MD30	−60	0.6	−60.6	OZF285	9330 ± 70	10,295–10,710 (10,535)	10529 ± 216
Marine molusks**	MRD28	−62	0.15	−62.2	OZE260	2935 ± 45	2440–3043 (2759)	2752 ± 290
	MRD31	−59	0.1	−59.1	OZF287	10,020 ± 160	10,565–11,695 (11,052)	11,069 ± 552
	MRD33	−68	0.1	−68.1	OZG237	1310 ± 40	683–1142 (905)	908 ± 234
	MDR30	−60	0.05	−60.1	OZG200	1655 ± 50	1011–1506 (1255)	1253 ± 244
	MRD32	−64	0.2	−64.2	OZG384	1820 ± 50	1209–1691 (1427)	1432 ± 240
	MRD31	−59	0.55	−59.6	OZG221	1930 ± 40	1304–1794 (1542)	1544 ± 252
	MRD31	−59	0.3	−59.3	OZG383	2290 ± 45	1705–2270 (1966)	1968 ± 280
	MRD28	−62	0.15	−62.2	OZE261	2600 ± 40	2080–2679 (2353)	2358 ± 310
	MRD33	−68	0	−68	OZG236	2875 ± 45	2356–2928 (2678)	2665 ± 290
	MRD31	−59	0.05	−59.1	OZG220	3770 ± 40	3486–4068 (3770)	3773 ± 290
	MRD31	−59	1.8	−60.8	OZG232	3810 ± 100	3460–4216 (3828)	3833 ± 380
	MRD30	−60	0.65	−60.7	OZE255	4310 ± 60	4188–4816 (4508)	4506 ± 330
	MRD33	−68	0.2	−68.2	OZG258	470 ± 50	0–366 (161)	167 ± 208
	MRD30	−60	0.3	−60.3	OZG381	4860 ± 50	4875–5484 (5212)	5206 ± 312
	MRD31	−59	0	−59	OZE262	6840 ± 50	7178–7588 (7397)	7393 ± 208
	MRD31	−59	0.55	−59.6	OZE256	6910 ± 80	7216–7689 (7459)	7456 ± 234
	MRD33	−68	0.2	−68.2	OZG259	700 ± 30	135–551 (378)	371 ± 202
	MDR31	−59	0.6	−59.6	OZG377	735 ± 35	150–620 (407)	400 ± 198

(Continued)

Table 3. (Continued)

Environment	Core code	Core water depth (m)	Sample core depth (m)	Sample relative to PMSL (m)	Lab. code	Conventional ^{14}C age (yr BP (1σ))	Calibrated ^{14}C age (cal. yr BP)	
							2σ age range (median)	Mean ± 2σ
	MRD28	−62	0	−62	OZE263	750 ± 60	149–637 (418)	411 ± 216
	MRD29	−60	0.05	−60.1	OZF283	820 ± 45	285–652 (482)	475 ± 198
	MRD33	−68	0.3	−68.3	OZG389	820 ± 50	281–656 (482)	475 ± 200
	MRD30	−60	0	−60	OZF284	8270 ± 60	8545–9205 (8865)	8864 ± 336
	MRD28	−62	0.5	−62.5	OZE257	9520 ± 89	10,142–10,782 (10,439)	10443 ± 328
	MRD32	−64	0.1	−64.1	OZG235	9700 ± 45	10,371–11,011 (10,663)	10,671 ± 312
	MRD32	−64	0	−64	OZF289	9705 ± 45	10,380–11,016 (10,670)	10,678 ± 312
	MRD29	−60	0.2	−60.2	OZE259	9810 ± 90	10,488–11,148 (10,810)	10,810 ± 346
	MRD28	−62	0.35	−62.4	OZG379	9920 ± 60	10,644–11,194 (10,932)	10,925 ± 294

*Non-marine.
**Marine.

Table 4. Previous published radiocarbon and luminescence ages from beach and chenier ridge system and bioherm deposits (a) Rhodes et al., 1980 and Rhodes, 1982; (b) Nanson et al., 2013; and, (c) Rosendahl, 2012 and Rosendahl et al., 2015).

a.

Location	Sample material	Lab. Code	Facies	Interface relative to PMSL (m)	Sample relative to PMSL (m)	Conventional ^{14}C age yr BP (1σ)	Calibrated ^{14}C age (cal. yr BP)	
							2σ age range (median)	Mean ± 2σ
Edward River	Shell Hash	ANU1690	BRdg	1	1.2	6400 ± 90	6629–7249 (6941)	6939 ± 322
Christmas Creek	Shell Hash	ANU1728	BRdg	0.3	1.75	1920 ± 120	1225–1900 (1540)	1547 ± 346
Christmas Creek	Shell Hash	ANU1732	BRdg	1.5	1.5	5370 ± 60	5561–6091 (5791)	5794 ± 262
Christmas Creek	Shell Hash	ANU1734	BRdg	1	1.25	3610 ± 70	3268–3889 (3575)	3578 ± 310
Christmas Creek	Shell Hash	ANU1735	BRdg	1	3.05	3110 ± 65	2710–3290 (2965)	2972 ± 294
Christmas Creek	Shell Hash	ANU1736	BRdg	0.75	3.25	3130 ± 65	2732–3297 (2988)	2994 ± 296
Edward River	*Anadara*	ANU1899	BRdg	0.5	2.1	690 ± 80	80–600 (365)	354 ± 250
Edward River	*Anadara*	ANU2057	BRdg	0.1	1.65	1240 ± 70	624–1109 (838)	844 ± 244
Edward River	Shell Hash	ANU2059	BRdg	0.25	1.75	3300 ± 85	2847–3510 (3192)	3187 ± 332
Edward River	Shell Hash	ANU2060	BRdg	0.55	1.2	3750 ± 80	3417–4089 (3749)	3752 ± 338
Edward River	Shell Hash	ANU2100	BRdg	0.8	1.5	6000 ± 100	6181–6816 (6481)	6486 ± 314
Edward River	*Anadara* and *Mactra*	ANU2101	BRdg	0.6	1	5760 ± 110	5891–6551 (6217)	6214 ± 334
Edward River	Shell Hash	ANU2102	BRdg	0.75	1.75	3430 ± 100	2967–3704 (3353)	3350 ± 364
Edward River	*Anadara*	ANU2103	BRdg	0	1.2	1880 ± 90	1231–1811 (1492)	1500 ± 296
Karumba	*Anadara*	ANU1740A	Chenier	2.75	4.75	5990 ± 90	6186–6776 (6470)	6474 ± 298
Pandanus Yard	Shell Hash	ANU1691	Chenier	2.75	5.4	5830 ± 100	5972–6621 (6297)	6295 ± 322
Karumba	*Anadara*	ANU1740C	Chenier	2.75	4	5780 ± 90	5922–6531 (6239)	6235 ± 306
Karumba	*Anadara* and *Mactra*	ANU1741	Chenier	2	4.4	4260 ± 100	4059–4819 (4437)	4435 ± 396
Karumba	*Mactra*	ANU1742	Chenier	2	2.6	3430 ± 60	3036–3645 (3354)	3350 ± 300
Karumba	*Mactra*	ANU1745	Chenier	1.5	1.95	1080 ± 60	507–911 (696)	702 ± 214
Pandanus Yard	*Mactra*	ANU1827	Chenier	2.35	3.5	2250 ± 60	1615–2240 (1917)	1919 ± 296
Karumba	*Anadara*	ANU1927	Chenier	1.6	2	1770 ± 70	1127–1671 (1379)	1383 ± 262
Karumba	*Mactra*	ANU1928	Chenier	2.25	2.75	2240 ± 65	1597–2240 (1905)	1907 ± 302
Pandanus Yard	*Mactra*	ANU1977	Chenier	1.65	3	680 ± 70	61–560 (358)	347 ± 242
Pandanus Yard	*Mactra*	ANU1998	Chenier	1.65	2.8	550 ± 80	0–444 (231)	232 ± 252
Christmas Creek	Shell Hash	ANU1730	ITM	1.25	1.25	5590 ± 250	5465–6644 (6042)	6045 ± 590
Christmas Creek	Shell Hash	ANU1733	ITM	0.5	0.5	5570 ± 120	5651–6335 (6019)	6014 ± 344
Christmas Creek	Shell Hash	ANU1737	ITM	0.5	0.5	3220 ± 70	2783–3379 (3094)	3094 ± 310
Karumba	*Anadara* and *Mactra*	ANU1743	ITM	1.5	1.5	3840 ± 140	3440–4350 (3874)	3880 ± 460
Edward River	*Anadara*	ANU1898	ITM	0.25	0.25	610 ± 70	0–494 (293)	283 ± 252
Christmas Creek	Shell Hash	ANU1729	STM	0.25	0.25	6160 ± 180	6240–7160 (6668)	6675 ± 472
Karumba	*Mactra*	ANU1744	STM	0.25	0.25	4540 ± 80	4448–5196 (4799)	4801 ± 368
Karumba	*Anadara* and *Mactra*	ANU1746	STM	−1.5	−1.5	3560 ± 70	3209–3829 (3514)	3517 ± 308

b.

Sample material	Lab. code (Core Code)	Core relative to PMSL (m)	Facies	Interface relative to PMSL (m)	Sample relative to PMSL (m)	^{14}C age BP (1σ)	Calibrated ^{14}C age (cal. yr BP)	
							Median cal. yr BP 2σ range	Mean cal. yr BP (2σ)
Mactra sp.	OZM484 (WP171)	0.35	BRdg/C	3.15	1.85	4900 ± 25	4973–5544 (5274)	5261 ± 294
OSL: chenier	AdGL12005 (WP71)	1.38	BRdg/C	3.97	1.4	N/A	N/A	400 ± 30
OSL: chenier	AdGL12003 (WP42)	0.75	Chenier/C	3.1	1.45	N/A	N/A	1520 ± 10

Table 4. (Continued)

b.

Sample material	Lab. code (Core Code)	Core relative to PMSL (m)	Facies	Interface relative to PMSL (m)	Sample relative to PMSL (m)	^{14}C age BP (1σ)	Calibrated ^{14}C age (cal. yr BP)	
							Median cal. yr BP 2σ range	Mean cal. yr BP (2σ)
Anadara antiquata	OZM487 (WP70)	0.90	Chenier	2.15	1.7	1905 ± 35	1287–1764 (1513)	1517 ± 244
Mactra sp.	OZM488 (WP70)	1.05	Chenier/B	2	1.7	1780 ± 30	1169–1617 (1386)	1391 ± 222
TL: chenier	W4324 (WP68)	1.2	Chenier/B	2.61	2.11	N/A	N/A	5700 ± 40
OSL: chenier	AdGL12004 (WP68)	1.2	Chenier/B	2.61	2.11	N/A	N/A	5580 ± 40
Mactra sp.	OZM491 (WP42)	2.40	ITM/DF	1.45	1.45	2140 ± 30	1525–2040 (1782)	1781 ± 258
Bivalve fragment	OZM492 (WP42)	4.35	ITM/DF	−0.5	−0.5	2410 ± 30	1846–2344 (2109)	2108 ± 264
Anadara antiquata	OZM489 (WP70)	2.20	ITM/DF	0.85	0.85	2355 ± 30	1800–2307 (2044)	2046 ± 266

c.

Location	Lab. Code	Facies	Interface relative to PMSL (m)	Sample relative to PMSL (m)	^{14}C age BP (1σ)	Calibrated ^{14}C age (cal. yr BP)	
						Median 2σ range	Mean cal. yr BP (2σ)
Guttapercha/ surface	Wk-23132	FBI	2.76	2.76	4426 ± 42	4370–4935 (4652)	4646 ± 282
Site 36	Wk-38402	FBI	1.34	1.34	4446 ± 30	4402–4941 (4674)	4669 ± 274
Site 12 (Surface)	Wk-23135	FBI	3.3	3.3	5866 ± 45	6092–6610 (6336)	6337 ± 246
Wurdukanhan East	Wk-23133	FBI	1.50	1.50	5142 ± 43	5296–5806 (5547)	5546 ± 254
Site 12	Wk-38404	FBI	3.37	3.37	5576 ± 34	5775–6264 (6029)	6027 ± 244
Site 80	Wk-38405	FBI	1.65	1.65	5899 ± 35	6157–6631 (6370)	6373 ± 234
Site 35	Wk-38406	FBI	1.39	1.39	5913 ± 41	6167–6641 (6384)	6389 ± 240
Site 35 (surface)	Wk-23136	FBI	1.4	1.4	5961 ± 45	6203–6679 (6435)	6439 ± 242
Site 35	Wk-23136	FBI	1.40	1.40	5961 ± 45	6203–6679 (6435)	6439 ± 242
Site 218	Wk-38403	FBI	1.47	1.47	6026 ± 32	6276–6737 (6503)	6505 ± 238
Site 1/A	Wk-38401	FBI	2.93	2.93	6146 ± 37	6385–6900 (6636)	6636 ± 260
Site 1	Wk-23134	FBI	1.50	1.50	6238 ± 47	6459–7021 (6747)	6748 ± 278
Site 1/B	Wk-38407	FBI	2.76	2.76	6246 ± 38	6475–7024 (6756)	7102 ± 270

3. The upper-most facies comprise a well-rounded, well-sorted quartz sand, with common to present pisoliths. Grains are well-frosted and iron-stained indicating reworking and sub-aerial exposure. Shell fragments are present, whole valves rare to present and heavily weathered. In places, this facies forms an organic-rich sand with thin (cm-scale) organic-rich humic layer in inter-dune swales. The facies is interpreted as the aeolian capping of the beach ridge system (BRdg/Ae). Archaeological materials have only been observed in this upper-most unit (Twaddle et al., 2017).

Intertidal and subtidal mangrove and mudflat deposits

Cores and trenches in supra-tidal mudflats on Bentinck Island that are now elevated above PMSL (max. elevation + 2.8 m above PMSL) intersected sediments associated with ITMs and mangrove deposits, overlying the heavily weathered Normanton Formation (Figure 5). Stratigraphic sections along two transects (at Durruru and Thundiy) revealed four facies.

1. The basal mottled dense clay representing the weathered Winton Formation (Figure 5).
2. In places (laterally discontinuous) medium-grained, mixed siliciclastic and carbonate muddy sand. Faunal assemblage includes common articulated and disarticulated estuarine and nearshore mollusks including bivalves species identified in beach ridge systems as well as *Tegillarca granosa, Lunulicardia hemicardium, M. hiantina*, and *Mactra* sp., as well as common gastropods *Pollia undosa, Cerithium coralium* and *T. telescopium.* The facies is interpreted as a transgressive facies (Tf). At Rukathi River, this facies contains densely packed, centimetre-thick, organic-rich interbeds, representing intertidal mangrove facies. Radiocarbon age determination returned ages of 8377 ± 232, 7635 ± 52 and 7086 ± 246 cal. yr BP (Table 5).
3. Organic-rich sub-rounded-to-rounded fine-to-medium-grained silty sand (quartz). Common to abundant estuarine and nearshore bivalves *T. granosa, L. hemicardium* and *M. hiantina*, as well as common gastropods *P. undosa, C. coralium* and *T. telescopium*. Radiocarbon age determinations on estuarine bivalves range from ca. 4000 to 1000 cal. yr BP (Table 5). Fine laminations are observed in pits and trench sections. This facies is interpreted as an ITM.
4. The upper-most facies comprises very fine-grained silty sand. Fine laminations are observed in pits and trench sections. Salt crusts and desecration structures are common at the surface. This facies is interpreted as the modern supra-tidal mudflat.

Beach-rock

Stratigraphic logging of coastal exposures of beach-rock deposits from Albinia, Bentinck and Sweers Islands resulted in the identification of five main facies (Figures 3, 5 and 6).

1. Lower Cretaceous Normanton Formation comprising lateritic bedrock and weathered siltstones, commonly forming wave-cut cliffs and platforms in coastal outcrop.

Table 5. Age determinations obtained for this study (for locations see Figure 1b).

Location	Sample material	Lab. code	Core code	Core elevation (m)	Sample core depth (m)	Facies	Sample relative to PMSL (m)	Facies interface relative to PMSL (m)	Conventional ^{14}C Age (yr BP)	Calibrated ^{14}C age (cal. yr BP)	
										2σ age range (median)	Mean ± 2σ
Bentinck (Rukathi River)	Peat	OZT523	RRB2	NA	N/A	Tf	0.32	0.32	6795 ± 35	7585–7681 (7636)	7635 ± 52
Bentinck (Rukathi River)	*Anadara* sp.	OZT524	RRB2–200	NA	N/A	Tf	0.4	0.4	7865 ± 30	8150–8601 (8377)	8377 ± 232
Bentinck (Rukathi River)	*Marcia hiantina*	OZT525	RRB2–230	NA	N/A	Tf	0.66	0.66	6535 ± 30	6830–7325 (7092)	7086 ± 246
Bentinck (Dururu)	*Striostrea mytiloides*	Wk–26684	DUR (surface)	N/A	N/A	FBI	2.11	2.11	4170 ± 42	3977–4614 (4308)	4306 ± 310
Bentinck (Dururu)	*Striostrea mytiloides*	Wk–28768	DUR (surface)	N/A	N/A	FBI	2.21	2.21	4717 ± 42	4779–5318 (5041)	5045 ± 292
Bentinck (Melbamelbari)	*Striostrea mytiloides*	Wk–38839	BS12 (surface)	N/A	N/A	FBI	1.75	1.75	4757 ± 24	4814–5333 (5089)	5087 ± 280
Albinia (South)	*Striostrea mytiloides*	OZT516	A5	N/A	N/A	FBI	2.7	2.7	5185 ± 25	5333–5849 (5598)	5597 ± 242
Sweers (North)	*Favia pallida*	Wk–39387	SE9	N/A	N/A	FBI	1.8	1.8	5652 ± 25	5879–6314 (6102)	6099 ± 230
Bentinck (Marralda)	*Marcia hiantina*	Wk–37071	MIR2.050	4.2	0.5	BRdg/BB	3.7	0.9	1539 ± 25	920–1330 (1138)	1133 ± 214
Bentinck (Marralda)	*Marcia hiantina*	Wk–37072	MIR2.230	4.2	2.3	BRdg/BB	1.9	0.9	1949 ± 25	1327–1808 (1563)	1564 ± 246
Bentinck (Marralda)	*Marcia hiantina*	Wk–37073	MIR10.120	3.8	1.2	BRdg/BB	2.6	1	1229 ± 25	641–1042 (825)	828 ± 204
Bentinck (Marralda)	*Gafrarium austral*	Wk–37074	MIR10.230	3.8	2.3	BRdg/BB	1.5	1	1494 ± 25	890–1297 (1096)	1093 ± 214
Bentinck (Marralda)	*Marcia hiantina*	OZT521	MIR10–255	3.8	2.55	BRdg/BB	1.25	1	3620 ± 25	3339–3850 (3584)	3587 ± 264
Bentinck (Marralda)	*Marcia hiantina*	OZT522	MIR13–153	3.5	1.53	BRdg/BF	1.97	2.2	4495 ± 30	4436–5011 (4730)	4729 ± 286
Bentinck (Wirrngaji)	*Mactra* sp.	OZT529	WIR2–90	4.1	0.9	BRdg/BB	3.2	> 3	1695 ± 30	1064–1523 (1299)	1299 ± 228
Bentinck (Wirrngaji)	*Gafrarium austral*	OZT530	WIR4–140	4.15	1.4	BRdg/BB	2.75	> 2.8	990 ± 30	452–814 (614)	619 ± 176
Bentinck (Wirrngaji)	*Marcia hiantina*	OZT531	WIR5–80	3.7	0.8	BRdg/BB	2.9	0.8	595 ± 30	0–475 (280)	271 ± 234
Bentinck (Wirrngaji)	*Marcia hiantina*	OZT532	WIR5–165	3.7	1.65	BRdg/BB	2.05	0.8	620 ± 30	60–496 (308)	296 ± 230
Bentinck (Wirrngaji)	*Mactra* sp.	OZT533	WIR5–230	3.7	2.3	BRdg/BB	1.4	0.8	655 ± 30	91–521 (342)	154 ± 192
Bentinck (Melbamelbari)	*Lumulicardia hemicardium*	Wk–38837	BS1–1a	NA	N/A	BRc/BF	2	2.4	4657 ± 29	4694–5275 (4965)	4973 ± 296
Sweers (North)	*Gafrarium pectinatum*	Wk–39388	SE10	NA	NA	BRc/BB	5	2.3	4786 ± 25	4842–5391 (5121)	5118 ± 282
Sweers (North)	*Gafrarium pectinatum*	Wk–38838	SE11	NA	N/A	BRc/BB	4	2.3	4656 ± 29	4692–5275 (4963)	4972 ± 296
Bentinck (Melbamelbari)	*Gafrarium pectinatum*	Wk–39385	BS4	NA	N/A	BRc/BF	2.88	2.4	3923 ± 25	3680–4275 (3976)	3977 ± 294
Bentinck (Melbamelbari)	*Gafrarium pectinatum*	Wk–39386	BS6	NA	N/A	BRc/BF	3.45	2.4	3902 ± 25	3648–4236 (3947)	3948 ± 294
Bentinck (Thundiy)	*Marcia hiantina*	Wk–37065	THU1.140	1.6	1.4	ITM	0.2	0.2	2721 ± 25	2259–2748 (2506)	2503 ± 262
Bentinck (Thundiy)	*Tegillarca granosa*	Wk–37066	THU4.170	1.6	1.7	ITM	−0.1	−0.1	1553 ± 25	928–1343 (1152)	1146 ± 214
Bentinck (Thundiy)	*Charma* sp.	Wk–37067	THU4.220	1.6	2.2	ITM	−0.6	−0.6	2331 ± 25	1774–2293 (2015)	2017 ± 264
Bentinck (Thundiy)	*Charma* sp.	Wk–37068	THU4.290	1.6	2.9	ITM	−1.3	−1.3	3670 ± 25	3380–3906 (3646)	3648 ± 268
Bentinck (Thundiy)	*Gafrariumaustrale*	OZT526	THU6–380	1.6	3.8	ITM	−2.2	−2.2	1435 ± 20	819–1257 (1039)	1039 ± 220
Bentinck (Thundiy)	*Marcia hiantina*	Wk–37069	THU7.140	1.6	1.4	ITM	0.2	0.2	4020 ± 25	3830–4399 (4108)	4108 ± 296
Bentinck (Thundiy)	*Marcia hiantina*	OZT527	THU11–140	1.6	1.4	STM	0.2	0.2	4145 ± 25	3969–4557 (4275)	4272 ± 294
Bentinck (Dururu)	*Gafrarium australe*	Wk–37070	DUR1A.170	2.54	1.7	STM	0.84	0.84	6038 ± 25	6285–6742 (6516)	6517 ± 236
Sweers (North)	U/Th: Coral – *Faviidae*	WZ08_47	SE6 (i)	NA	N/A	Ae	6.1	6.1	N/A	N/A	5973 ± 14
Sweers (North)	U/Th: Coral – *Faviidae*	WZ08_48	SE6 (ii)	NA	N/A	Ae	6.1	6.1	N/A	N/A	5878 ± 76
Sweers (North)	U/Th: Coral – *Faviidae*	WZ08_49	SE1 (i)	NA	N/A	Ae	6.1	6.1	N/A	N/A	5706 ± 11
Sweers (North)	U/Th: Coral – *Faviidae*	WZ08_50	SE1 (ii)	NA	N/A	Ae	6.1	6.1	N/A	N/A	5713 ± 13
Sweers (North)	Coral – *Faviidae*	Wk–40373	SE6 (i)	NA	N/A	Ae	6.1	6.1	5578 ± 20	5789–6264 (6031)	6029 ± 236
Sweers (North)	Coral – *Faviidae*	Wk–40374	SE6 (ii)	NA	N/A	Ae	6.1	6.1	5574 ± 20	5785–6260 (6027)	6025 ± 238
Sweers (North)	Coral – *Faviidae*	Wk–40375	SE1 (i)	NA	N/A	Ae	6.1	6.1	5487 ± 20	5679–6175 (5925)	5926 ± 256
Sweers (North)	Coral – *Faviidae*	Wk–40376	SE1 (ii)	NA	N/A	Ae	6.1	6.1	5520 ± 20	5713–6205 (5966)	5966 ± 252

Table 6. Relative abundance of faunal elements relative to facies associations. Habitat information from Hodgson (1998) and Carpenter and Niem (1998). *a* = absent; *R* = rare; P = present; *C* = common; *VC* = very common; *F* = fragments and/or shell hash.

	Faunal element	Original habitat	Facies			
			Trans gressive facies	Intertidal facies	Beach-rock facies	Beach ridge system
Bivalves	*Tegillarca granosa (Anadara granosa)* Linnaeus, 1758	Common on muddy to muddy sand substrates, mainly in protected bays, estuaries, and mangroves environments. Intertidal (optimal water depths of 1–2 m either side of mid-tide), inhabiting environments with relatively low salinity.	*C (F-C)*	*VC*	*P*	*P (F-C)*
	Chama pacifica Broderip, 1834	Attached to corals, rocks, and pebbles. Littoral and sublittoral to a depth of 30 m.	*P*	*C*	*P*	*P*
	Circe scripta Linnaeus, 1758	Sandy substrates in the intertidal and shallow subtidal to a depth of about 20 m.	*P*	*C*	*P*	*a*
	Fragum hemicardium Linnaeus, 1758	Common in intertidal sandy substrates associated with sandflats of sheltered bays.	*C*	*VC*	*C*	*P*
	Gafrarium pectinatum Röding, 1798	Sandy substrates in intertidal and subtidal environments to a depth of ca. 30 m.	*VC*	*VC*	*C (F-C)*	*P-C*
	Lunulicardia hemicardium Linnaeus, 1758	Abundant in intertidal sandflats of sheltered bays with a depth range of 0–5 m.	*VC*	*C*	*C*	*R*
	Mactra maculata Gmelin, 1791	Fine sandy substrates in intertidal and subtidal environments (up to 60 m water depth).	*C*	*C*	*C (F-C)*	*P-C*
	Marcia hiantina (Katelysia hiantina) Lamarck, 1818.	Sandy to silty substrates in sheltered intertidal areas to subtidal up to 20 m water depth.	*C*	*C*	*P*	*R*
	Geloina erosa Lightfoot, 1786	Muddy substrates in fresh and brackish waters associated with mangrove swamps and estuaries. Can survive sub-aerial exposure for a few days.	*P*	*P*	*a*	*a*
	Saccostrea cucullata Born, 1778	Attached to various hard substrates in the intertidal zone (max. depth 5 m) associated with estuarine and mangrove environments.	*VC*	*a*	*a*	*a*
Gastropods	*Pollia undosa (Cantharus undosus)* Linnaeus, 1758	Intertidal on rocky or sandy substrates, also found associated with dead corals, in reef areas.	*P*	*C*	*a*	*a*
	Cerithium coralium Kiener, 1841	Found in the upper tidal zone (mid-to-high-tide) mudflats of estuarine and mangrove areas.	*P*	*C*	*C (F-C)*	*R*
	Clypeomorus batillariaeformis Habe and Kosuge, 1966	Sandy substrates in the intertidal zone associated with reef flats and estuarine environments.	*P*	*P*	*R*	*a*
	Littoraria scabra Linnaeus, 1758	Found attached to trees, roots and pneumatophores at the seaward edge of mangrove environments. Can also be found on sandy shores and on sheltered rocky intertidal environments.	*P*	*C*	*a*	*a*
	Rhinoclavis vertagus Linnaeus, 1758	Abundant on sandy substrates in intertidal and sub-tidal environments to a depth of ca. 13 m.	*P*	*P*	*R*	*R*
	Terebralia sulcata Born, 1778	Common on mudflats in estuaries and mangrove environments, often attached to pneumatophores and roots of the trees.	*P*	*C*	*P*	*R*
	Telescopium telescopium Linnaeus, 1758	Abundant in mangrove areas and on intertidal mudflats in saline or highly brackish environments.	*VC*	*VC*	*C*	*P-C*
Corals	*Acropora formosa* (Dana, 1846)	Often dominate large areas of lagoon in shallow and intermediate depths.	*VC*	*a*	*P*	*a*
	Acropora humilis (Dana, 1846)	Found on exposed reefs throughout its range in shallow to intermediate depths.	*C*	*a*	*a*	*a*
	Acropora palifera (Lamarck, 1816)	Common in shallow to intermediate depths and wave-washed environments.	*VC*	*a*	*a*	*a*
	Favia favus (Forsskål, 1775)	Found at all depths	*VC*	*a*	*P*	*a*
	Heliopora coerulea (Pallas, 1766)	Most common in shallow water.	*C*	*a*	*a*	*a*
	Pectinia lactuca (Pallas, 1766)	Common from below the reef flat to the limit of coral growth.	*C*	*a*	*a*	*a*
	Platygyra daedalea (Ellis and Solanader, 1786)	Colonies commonly grow to 1 m diameter or more and are found at all depths.	*C*	*a*	*a*	*a*

2. A laterally discontinuous unit ranging from a few centimetres to 30 cm thick. This facies comprises coral rubble in a medium-to-very-coarse-grained sand matrix and reworked shelly rubble with grainstone or boundstone texture and a sharp unconformable contact with the lateritic bedrock. This unit includes fragmented and reworked whole corals (*Favia favus* and *Acropora* sp.), abundant gastropods (*T. telescopium*) and bivalves (*G. australe*). Present to

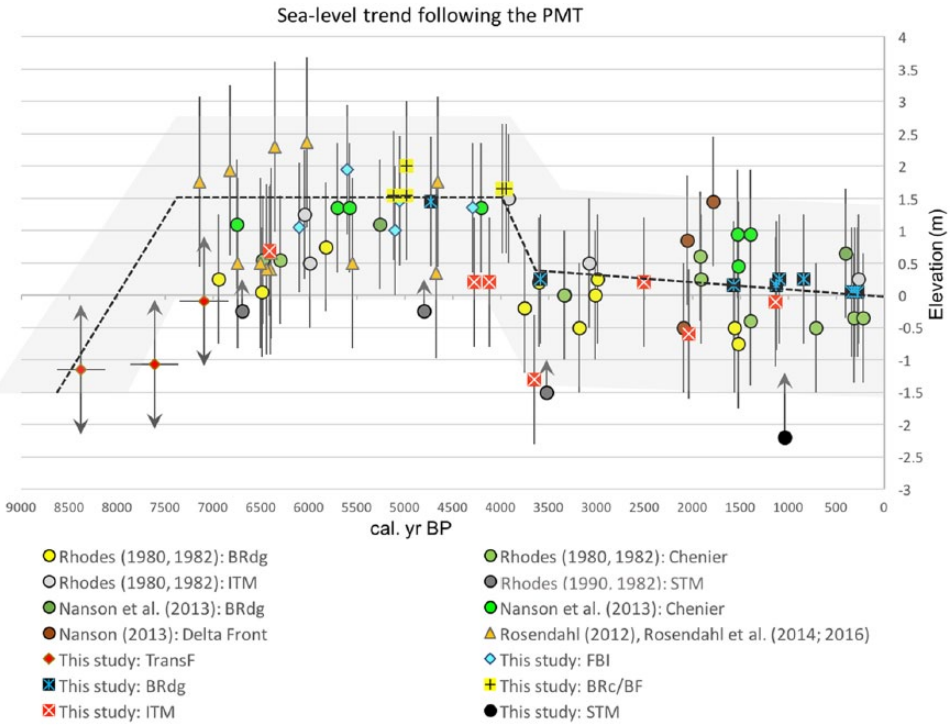

Figure 7. Revised Holocene sea-level curve for the southern Gulf of Carpentaria 10 ka–present. Sea-level curve representing line of best fit through the data points; grey hash represents the averaged vertical error of sea-level proxies and incorporates age determination errors.

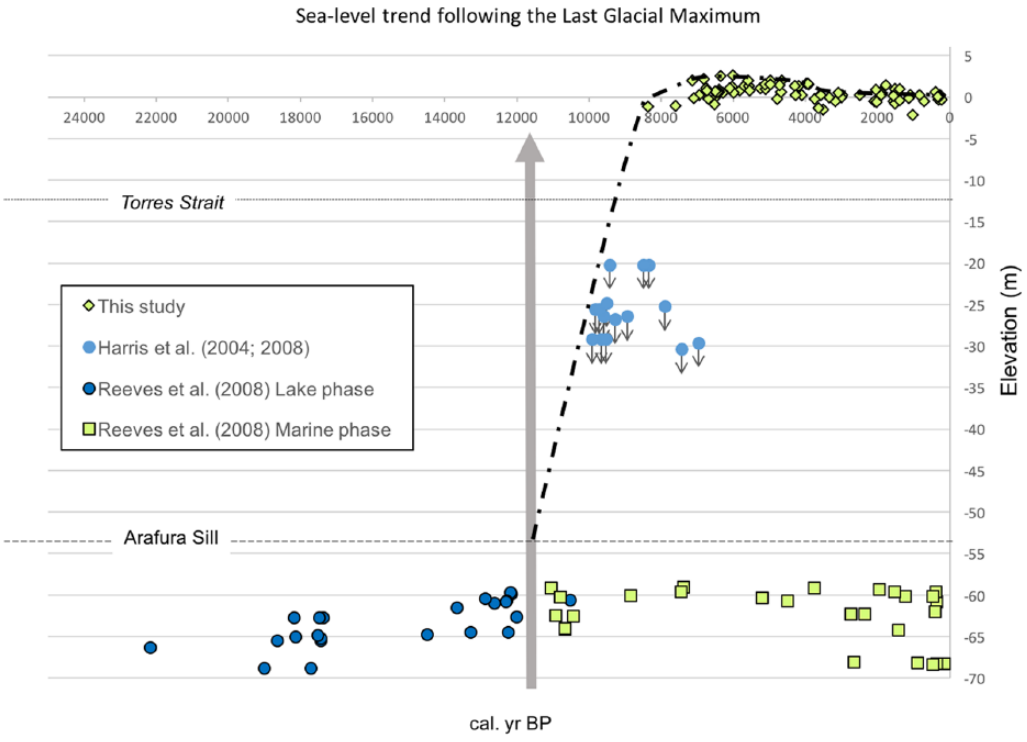

Figure 8. Revised Holocene sea-level curve for the southern Gulf of Carpentaria 22 ka–present.

common *in situ* coral occur at the base of the coral rubble facies. The facies is interpreted as transgressive facies (coral/TF). Radiocarbon age determinations could not be obtained on *in situ* coral due to recrystallization, however radiocarbon and U-Th ages from reworked coral do provide an age constraint of ca. 6000 cal. yr BP (Table 5; Figures 3, 5 and 6).

3. Consolidated beach-rock deposits unconformably overlying the lateritic bedrock. The facies is characterized by a mixed siliciclastic and bioclastic sediment with individual units fining-up from gravel and coarse-grained grainstone to medium-grained grainstone. Tabular forest beds with an east-west strike and dips varying between horizontal to ~25° to the south (seaward) are well-preserved. Faunal elements within this facies include fragmented abundant gastropods (*Terebralia* sp., *Calliostoma* sp.) and bivalves (*G. pectinatum, G. australe, L. hemicardium*). The facies is interpreted as a beach-face facies (BRc/BF; 5 and 6).
4. Up sequence the BRc/BF facies grades to a poorly-consolidated beach-rock characterized by a graded coarse-grained

grainstone, fining-up to a fine-grained grainstone. The facies is characterized by low angle planar bedding with a southeast-northwest strike and a northeast (landward) dip angle of 11°–28°. Faunal elements include very abundant fragmented gastropods (*Terebralia* sp., *Calliostoma* sp.) and bivalves (*G. pectinatum, G. australe, L. hemicardium*). The facies is interpreted as a back-beach facies (BRc/BB). Radiocarbon age determinations from this facies range from 5100 to ca. 4000 cal. yr BP, Table 4, 5, and 6).

5. *Aeolianite facies*. The aeolianite deposits are partially consolidated very fine-to-medium-grained, poorly sorted, sub-angular-to-sub-rounded siliciclastic and bioclastic sediments. The aeolianite facies is a laterally variable unit reaching up to 2 m thick in some sections, with a sharp basal contact with the underlying beach-rock and a distinct karstic weathering. Faunal elements included rare-to-present fragmented bivalves (*G. pectinatum, G. australe, L. hemicardium*) and very rare-to-rare gastropods (*Terebralia* sp., *Calliostoma* sp.). Within the aeolianite facies corals (*F. pallida, L. phyrgia, Heliopora coerulea, C. serailia*) transported from adjacent palaeo-reefs ranging in size from 6 to 13 cm occur as reworked and imbricated concentrated bands.

Intertidal erosional indicators

Wave-cut notches and benches eroded into the soft weathered lateritic sandstones and siltstones of Normanton Formation are common geomorphological features on the South Wellesley Islands. These erosional features are commonly overlain by Holocene deposits and/or aeolian dunes containing archaeological material. These features are assumed to represent the elevation of the Holocene highstand eroded into the soft bedrock and/or moderately consolidated beach-rock. The wave-cut bench surveyed on Fowler Island extends up to 4 m horizontally, eroded into the Normanton Formation. The wave-cut benches surveyed on Albinia and Sweers Islands extends between 10 and 20 m horizontally, eroded into beach-rock deposits (Figure 6). These wave-cut features have an elevation (IM) of between + 1.5 and + 3.5 m (Avg. elevation = + 2 m). On Bentinck Island, a wave-cut notch of ca. + 1.5 m in height and 1.5 m in depth occupies the upper limits of the elevated intertidal mudflats at Rukathi River at an elevation of between + 1.5 and + 2.5 m above PMSL indicating a contemporary sea-level (IM) of ca. 2 m above PMSL (Figures 5 and 6).

Encrusting organisms and oyster bioherm

On both Bentinck and Albinia Island *S. mytiloides* occur as small accumulations attached to elevated wave-cut benches and within partially consolidated deposits. On Bentinck Island, *in situ S. mytiloides* were recovered at the landward margin of the extensive intertidal and supra-tidal mudflats at Dururu. Age determinations on *in situ S. mytiloides* recovered from the lowest elevation returned a radiocarbon age of 4306±310 cal. yr BP (IM + 2.11 m, Table 5). At the upper limit, *in situ S. mytiloides* returned a radiocarbon age of 5045±292 cal. yr BP (IM + 2.21 m; Table 5). Encrusted *in situ S. mytiloides* collected from the raised notches on Albinia Island and the coral rubble facies on Bentinck Island returned radiocarbon age determinations of 5998 ± 265 at + 1.95 m, and 5118±282 cal. yr BP at + 1 m respectively (Table 5).

Discussion: Revised sea-level history for the southern Gulf of Carpentaria

Utilizing results from previous studies and from this research a detailed history of Holocene sea-level change has been constructed for the southern Gulf of Carpentaria. The sea-level history has been divided into three main phases with each phase characterized by a specific set of climate conditions and sea-level elevations, which significantly influenced coastal landscape evolution.

Phase 1: PMT of the Gulf region (ca. 12,000 to 7000 cal. yr BP)

The compilation of previous research, with results from this study, indicate that sea-level rose from −53 m (depth of the Arafura Sill) ca. 11,700 years ago to ca. –25 m by 9800 years ago (Figure 8). Based on results from *in situ S. mytiloides* and transgressive deposits sea-level attained PMSL by 7700 years ago and continued to rise to an elevation of between 1.5 and 2 m by 7000 years ago (Figures 7 and 8). The revised sea-level history contrast with previous research that suggest a much higher sea-level of ca. 2.5 m above PMSL ca. 6400 cal. yr BP before falling to its present level (Chappell et al., 1982; Rhodes, 1982; Rhodes et al., 1980). Results from the southern Gulf of Carpentaria also place the culmination of the most recent PMT 2000 to 1500 years earlier than previously reported (Chappell et al., 1982; Rhodes, 1982; Rhodes et al., 1980).

While coastal erosional features are difficult to date, the wave-cut notches and benches surveyed in the South Wellesley Islands provide evidence to support the hypothesis of the earlier culmination of the most recent PMT. For example, at the landward limit, the erosional bench on Fowler Island is overlain by Holocene dune sediments that contain evidence of Aboriginal occupation dated to between 132 cal. yr BP (431 ± 25 BP, Wk-34781) and 934 cal. yr BP (1,337 ± 25 BP, Wk-34783). The weathered Normanton Formation is a soft laterite and easily eroded, making it unlikely that wave-cut features are remnants of previous interglacials. Using the modern platform as an analogue the elevated wave-cut notch and benches represent an elevated sea-level of 2.25 ± 1.5 m above PMSL, most likely formed during the culmination of the most recent PMT (Figures 5 and 6)

A more accurate elevation and age control for sea levels during the most recent PMT has been obtained utilizing fixed biological indicators. On Mornington Island, 12 *S. mytiloides* bioherm clusters were documented by Rosendahl et al. (2015). The bioherm clusters are characterized by mono-specific accumulations of *S. mytiloides* that exhibit excellent valve preservation and an abundance of articulated valves representing *in situ* accumulation. Radiocarbon age determinations from the bioherms fall between 7000 and 4600 cal. yr BP at elevations between 1.34 and 3.3 m above PMSL (Table 5). The age determinations obtained by Rosendahl et al. (2015) indicate that the coastline was adjacent to the bedrock margins by ca. 7000 cal. yr BP and embayments represented both inter- and subtidal environments characterized by sea-grass beds and mangrove communities, and not a supra-tidal mudflat as it is today. Age determinations on *in situ S. mytiloides* from this study are consistent with Rosendahl et al. (2015). *S. mytiloides* attached to wave-cut features from Albinia, Sweers and Bentinck Islands indicate that sea-level was between +1 and +1.95 (IM) above PMSL by 6100 cal. yr BP.

Further evidence constraining the timing of the culmination of the most recent PMT was recovered from transgressive deposits associated with a basal coral rubble deposit underlying late Holocene deposits. An *in situ S. mytiloides* within the basal coral facies indicates that the transgressive facies was deposited before 5100 cal. yr BP. U-Th and radiocarbon age determinations on the reworked corals in storm deposits preserved within the overlying aeolian facies indicate that coral communities would have been in growth position near present sea-level ⩾6000 cal. yr BP, and subsequently been incorporated into the overlying aeolian facies.

Similar evidence for the timing and elevation of the culmination of the most recent PMT were obtained from transgressive mangrove deposits. Since mangrove-related sedimentary deposits are intertidal, deposition at a particular level in the past can provide an indication of the position of former sea-level (Jones et al.,

1979; Lewis et al., 2013; Sloss et al., 2005, 2007; Thom and Roy, 1983, 1985; Woodroffe, 1988). On the Wellesley Islands, transgressive mangrove muds occur beneath intertidal mudflats which records both changes of sea-level and coastal landscape response to such changes. Within the transgressive deposits at Rukathi, a dense shell bed was dated at 8377 ± 227 cal. yr BP. This unit has sharp upper and basal contacts with abundant disarticulated and hydro-dynamically sorted bivalves. This is most likely a storm-redeposited bed within an early forming mangrove fringe. The age determinations from this unit indicate that sea-level was close to present ca. 8300 years ago and re-worked material into the nearshore zone. Additional results from transgressive deposits indicate that sea-level attained PMSL between 7611 ± 187 and 7086±246 cal. yr BP (Table 5; Figure 7).

Phase 2: Mid-Holocene sea-level highstand (ca. 7000–4000 cal. yr BP)

Following the culmination of the most recent PMT sea-level remained at an elevation of between 1 and 2 m above PMSL during the Holocene highstand which lasted until ca. 4000 cal. yr BP. For example, results from the landward limit of the Dururu claypan show that *in situ S. mytiloides* clusters accumulated between 5050 ± 217 cal. yr BP (upper limit of oyster bed + 1.46 m) and 4295 ± 315 cal. yr BP (lower limit of oyster bed + 1.36 m). It was also during this phase of elevated sea-level that resulted in the formation of beach-rock successions. Environmental conditions were favourable with increased temperatures and precipitation during the mid-Holocene climate optimum (Shulmeister, 1999; Shulmeister and Lees, 1992), facilitating dissolution and precipitation of carbonate material, resulting in the formation of beach-rock immediately following the culmination of the most recent PMT. Results from this research identified the facies interface between the shallow seaward dipping and landward dipping beach facies to be between 2 and 2.4 m above PMSL. Radiocarbon age determinations from reworked bivalves provide a maximum age for the deposit and indicate that they were forming ⩾ 5100 years ago, and abruptly ceased formation shortly after 4000 cal. yr BP (Figures 7 and 8; Table 5). The cessation of beach-rock formation is most likely associated with a decrease in effective precipitation and temperature after ca. 5000 years ago (Shulmeister, 1999; Shulmeister and Lees, 1992), and a falling sea-level from 4000 cal. yr BP resulting in a decrease in sediment supply.

Increased precipitation and temperature combined with elevated sea levels during the Holocene sea-level highstand also had a significant influence on chenier and beach ridge initiation and development. The beach ridge system at Marralda shows a general age progression from the older landward dunes to the younger seaward dunes with results indicating an initial phase of dune building associated with the culmination of the most recent PMT ca. 6700 to 6000 cal. yr BP (Figure 7). At Wirrngaji the older inland dune formed a stationary/aggradational barrier before transitioning into younger seaward dunes. Initial increased dune activity would have been facilitated by increased sediment supply associated with higher effective precipitation, erosion and sediment supply, combined with elevated sea levels of between 1.5 and 2 m above PMSL.

Results from this study are consistent with similar geomorphological evidence on Groote Eylandt, the Cobourg Peninsula (northeast of Darwin) and Cape Flattery on Cape York Peninsula, that indicate coastal dune initialization and stabilization occurring between 6000 and 4000 years ago (Lees, 1987; Lees et al., 1990; Shulmeister and Lees, 1992). It was this phase of elevated sea levels associated with the highstand that resulted in the initiation and development of mangrove and intertidal flats.

Our revised sea-level curve for the southern Gulf of Carpentaria is similar to results obtained on the southeast coast of Australia by Sloss et al. (2005, 2007), which identified a rapidly rising sea-level following the LGM and a culmination of the PMT of + 1.5 m ca. 7400. A full review of Holocene sea-level around the Australian continental margin is provided by Lewis et al. (2013) which shows that, in general, sea-level around the coastal margin of Australia attained PMSL between 8000 and 7400 cal. yr BP, with an elevation of between 1 and 2 m above PMSL. The similarities of the initial peak in sea-level during the most recent PMT observed in the Gulf of Carpentaria and other Australasian sites may suggest that eustatic sea-level due to melt-water influx during deglaciation resulted in regionally similar early Holocene sea-level history in far-field sites in the Australasian region.

Phase 3: Regression from mid-Holocene sea-level highstand to PMSL (ca. 4,000 cal. yr BP – present)

Results from this study indicate that sea-level remained above PMSL until a regression from ca. 4000 cal. yr BP reaching within ± 0.5 m of PMSL by ca. 3500 cal. yr BP (Figure 7). Rhodes (1982) and Chappell et al. (1982) attribute the Holocene relative sea-level fall within the Gulf of Carpentaria from ca. 6000 cal. yr BP to subsidence in northeastern Australia due hydro-isostatic loading. The subsidence in the central basin resulted in a forced regression due to uplift of between 0.2 and 1.4 m for western Cape York, and between 1.7 and 3.1 m in the Flinders-Leichhardt region (Chappell et al. 1982; Figure 1). However, Jones and Torgersen (1988) concluded that due to the continuous net accumulation of sediment on the Arafura Sill and within the central basin it is unlikely that significant uplift occurred, and the effects of subsidence would also have been minimal due to continuous lacustrine conditions during the last glacial phase.

Results indicate a potential hiatus in coastal accretion between 3000 and 1900 cal. yr BP. Again, results from this research are consistent with research by Lees (1987), Lees et al. (1990) and Shulmeister and Lees (1992) who identified a sharp decline in precipitation after 3700 cal. yr BP associated with an onset of a modern-style ENSO and characterized by increase in climatic variability. The decrease in precipitation and increased climate variability between 3700 and 1900 years ago would have resulted in reduced erosion and transport of sediment to the Gulf, which retarded coastal progradation. Indeed, Nanson et al. (2013) and Lane et al. (2017) identified a pronounced ca. 100 km long ca. 2000 year palaeoshorelines within the Mitchell and Nassau deltas, which demonstrate this hiatus in shoreline progradation and the subsequent down-stepping of these systems in response to falling sea-level. Research by Moss et al. (2015) on Bentinck Island also identified that coastal wetland development occurred from ca. 2400 to 500 years ago, consistent with a sea-level close to present levels and a hiatus in sediment supply to the coastal fringe.

A more recent phase of dune formation (Phase 2) and coastal progradation from 1900 cal. yr BP (Figures 4 and 7) is also identified in this study. This second phase of ridge activity is characterized by lower elevations of dune and chenier ridges (Figures 4 and 7). In contrast to higher dune accretion of Phase 1, this phase of dune and chenier development is characterized by accelerated coastal progradation with progradation of approximately 400 m at both Marralda and Wirrngaji. The rapid progradation, contrast in dune morphology and the presence of mangrove and freshwater indicates a shift from local controls on dune development of Phase 1 to more regional factors such as climate change. This is also consistent with palynological research on Bentinck Island showing an expansion of the mangrove fringe and the establishment of freshwater swamps in inter-dune swales (Moss et al., 2015). The increased sediment supply and recent phase of coastal dune building provided protection for expanding mangrove and freshwater swamps and most are likely associated with an increase in effective precipitation (Lees et al., 1990; Shulmeister and Lees, 1992).

The increased coastal dune and beach ridge activity from ca. 1900 years ago identified in this study and the region by Shulmeister and Lees (1992), Shulmeister (1999), Nanson et al. (2013) and Lane et al. (2017) is not restricted to northern Australia, but is a South Pacific-wide phenomenon. Research by Moy et al. (2002) from lacustrine deposits in Laguna Pallcacocha southern Ecuador also show a peak in ENSO amplitude occurring ca. 2000–1000 cal. yr BP, which then decreases towards modern times. Similarly, research in El Junco Crater Lake in the Galápagos Islands indicates increased precipitation and greatest ENSO variance in the Holocene occurred between 2000 ± 100 and 1500 ± 70 cal. yr BP (Conroy et al., 2008). When placed into a wider regional context results from this study show that coastal landscape evolution in the tropical north of Australia was not only dependent on sea-level change but also show a direct correlation with Holocene climate variability. Specifically, the formation and preservation of beach-rock deposits, intertidal successions, beach and chenier ridge systems hold valuable sea-level and Holocene climate proxies that can contribute to the growing research into lower latitude Holocene sea-level and climate histories.

Conclusion

The compilation of results from previous research, and results of this research, indicate that rising sea levels beached the Arafura Sill ca. 11,700 cal. yr BP, with full marine conditions attained in the Gulf of Carpentaria by 10,500 cal. yr BP. Inundation resulted in coral reef development between 10,500 and 9500 cal. yr BP at elevations between 20 and 30 m below PMSL. Sea-level continued to rise to PMSL ca. 7700 cal. yr BP and attained a highstand of between + 1.5 and + 2 m by ca. 7000 cal. yr BP. Sea-level highstand remained between + 1.5 and + 2 m above PMSL until ca. 4000 cal. yr BP, followed by a rapid regression to near present by ca. 3500 cal. yr BP. When placed into context with other far-field sites in the Australian region, the sea-level history observed in the southern Gulf of Carpentaria calls into question the role of localized hydro-isostasy on relative sea-level history in the region. The similarities between the Gulf of Carpentaria and the wider Australian region provides additional data for ongoing research into the Holocene eustatic sea-level change during the culmination of the most recent PMT.

This research highlights the interconnection between sea-level change, Holocene climate variability and coastal landscape evolution. Specifically, culmination of the most recent PMT and Holocene sea-level highstand (7700–4000 years ago) and a corresponding period of increased precipitation and temperature during the Holocene climate optimum resulted in conditions suitable for the deposition and formation of beach-rock and the initiation of the first phase of dune and chenier ridge development occurred. Coastal progradation of beach and chenier ridges occurred associated with a rapid fall in sea-level between 4000 and 3700 years ago, and again from 1900 years ago to the present, strongly influenced by climate variability associated with the onset and intensification of the ENSO.

Acknowledgements

We acknowledge Kaiadilt traditional owners of the South Wellesley Islands as partners in this research. The Kaiadilt Aboriginal Corporation collaborated in establishing the research framework for this project. We extend a special thanks to Duncan Kelly and Lincoln Steinberger for assistance in the field. Thanks go to Tex and Lyn Battle for assistance with logistics. Work on this paper was undertaken while S.U. was visiting as an Honorary Fellow in the School of Social Sciences, The University of Western Australia. This paper is a contribution to the International Quaternary Association (INQUA) working group on 'Coastal and Marine Processes' and SHAPE (Southern Hemisphere assessment of palaeo-environments). We also thank Dr. Amy Dougherty and an anonymous review for constructive comments that improved this manuscript.

Funding

This project was supported under the Australian Research Council's Discovery Projects (project numbers DP120103179 and DP0663047) and Australian Institute of Nuclear Sciences and Engineering (ALNGRA13017, ALNGRA15513) funding schemes. S.U. is the recipient of an Australian Research Council Future Fellowship (FT120100656). We acknowledge the financial support from the Australian Government for the Centre for Accelerator Science at ANSTO through the National Collaborative Research Infrastructure Strategy (NCRIS).

ORCID iD

Craig R Sloss https://orcid.org/0000-0001-8694-6822

References

Augustinus P (1989) Cheniers and chenier plains: A general introduction. *Marine Geology* 90: 219–229.

Augustinus P, Hazelhoff L and Kroon A (1989) The chenier coast of Suriname: Modern and geological development. *Marine Geology* 90: 269–281.

Baker RGV and Haworth RJ (1997) Further evidence from relic shellcrust sequences for a late Holocene higher sea level for eastern Australia. *Marine Geology* 141: 1–9.

Baker RGV and Haworth RJ (2000a) Smooth or oscillating late Holocene sea-level curve? Evidence from cross-regional statistical regressions of fixed biological indicators. *Marine Geology* 163: 353–365.

Baker RGV and Haworth RJ (2000b) Smooth or oscillating late Holocene sea-level curve? Evidence from the palaeo-zoology of fixed biological indicators in east Australia and beyond. *Marine Geology* 163: 367–386.

Baker RGV, Haworth RJ and Flood PG (2001a) Inter-tidal fixed indicators of former Holocene sea levels in Australia: A summary of sites and a review of methods and models. *Quaternary International* 83–85: 257–273.

Baker RGV, Haworth RJ and Flood PG (2001b) Warmer or cooler late Holocene marine palaeoenvironments? Interpreting southeast Australian and Brazilian sea-level changes using fixed biological indicators and their $d^{18}O$ composition. *Palaeogeography, Palaeoclimatology, Palaeoecology* 168: 249–272.

Baker RGV, Haworth RJ and Flood PG (2005) An oscillating Holocene sea-level? Revisiting Rottnest Island, Western Australia, and the Fairbridge Eustatic hypothesis. *Journal of Coastal Research* 42: 3–14.

Beaman R, Larcombe P and Carter RM (1994) New evidence for the Holocene sea-level high from inner shelf central Great Barrier Reef, Australia. *Journal of Sedimentary Research* 64: 881–885.

Benac C, Juracic M and Bakran-Petricioli T (2004) Submerged tidal notches in the Rijeka Bay NE Adriatic Sea: Indicators of relative sea-level change and of recent tectonic movements. *Marine Geology* 212: 21–33.

Bronk Ramsey C (2009) Bayesian analysis of radiocarbon dates. *Radiocarbon* 51: 337–360.

Brooke BP, Lee R, Cox M et al. (2008) Rates of shoreline progradation during the last 1700 years at Beachmere, southeastern Queensland, Australia, based on optically stimulated luminescence dating of beach ridges. *Journal of Coastal Research* 24(3): 640–648.

Brooke BP, Nichol SL, Huang Z et al. (2017) Palaeoshorelines on the Australian continental shelf: Morphology, sea-level relationship

and applications to environmental management and archaeology. *Continental Shelf Research* 134: 26–38.

Bureau of Meteorology (BOM) (2016) Monthly climatic statistics for Sweers Island, Queensland. Available at: http://www.bom.gov.au/climate/averages/tables/cw_029139.shtml (accessed 29 April 2016).

Carpenter KE and Niem VH (eds) (1998) *The Living Marine Resources of the Western Central Pacific. Volume 1. Seaweeds, Corals, Bivalves and Gastropods* (FAO species identification guide for fishery purposes). Rome: FAO, pp. 1–686.

Chappell J, Chivas A, Wallensky E et al. (1983) Holocene palaeo-environmental changes, central to north great Barrier Reef inner zone. *BMR Journal of Australian Geology and Geophysics* 8: 223–235.

Chappell J, Rhodes EG, Thom BG et al. (1982) Hydro-isostasy and the sea-level isobase of 5500 B.P. in North Queensland, Australia. *Marine Geology* 49: 81–90.

Chivas AR, Garcia A, van der Kaars S et al. (2001) Sea-level and environmental changes since the last interglacial in the Gulf of Carpentaria, Australia: An overview. *Quaternary International* 83–85: 19–46.

Church JA and Forbes AMG (1981) Non-linear model of the tides in the Gulf of Carpentaria. *Australian Journal of Marine and Freshwater Research* 32: 685–697.

Clark TR, Zhao J-X, Feng Y-X et al. (2012) Spatial variability of initial $^{230}Th/^{232}Th$ in modern *Porites* from the inshore region of the Great Barrier Reef. *Geochimica et Cosmochimica Acta* 78: 99–118.

Conroy JL, Overpeck JT, Cole E et al. (2008) Holocene changes in eastern tropical Pacific climate inferred from a Galápagos lake sediment record. *Quaternary Science Reviews* 27: 1166–1180.

Day RW (1983) *Queensland Geology: A Companion Volume to the 1: 2,500,000 Scale Geological Map (1975)*. Brisbane: Geological Survey of Queensland.

Desruelles S, Fouache E, Ciner A et al. (2009) Beachrocks and sea level changes since Middle Holocene: Comparison between the insular group of Mykonos-Delos-Rhenia (Cyclades, Greece) and the southern coast of Turkey. *Global and Planetary Change* 66: 19–33.

Dougherty AJ (2014) Extracting a record of Holocene storm erosion and deposition preserved in the morphostratigraphy of a prograded coastal barrier. *Continental Shelf Research* 86: 116–131.

Dougherty AJ and Dickson ME (2012) Sea level and storm control on the evolution of a chenier plain, Firth of Thames, New Zealand. *Marine Geology* 307–310: 58–72.

Engelhart SE, Horton BP, Douglas BC et al. (2009) Spatial variability of late Holocene and 20th century sea-level rise along the Atlantic coast of the United States. *Geology* 37: 1115–1118.

Fink D, Hotchkis M, Hua Q et al. (2004) The ANTARES AMS facility at ANSTO. *Nuclear Instruments and Methods in Physics Research Section B* 223–224: 109–115.

Geocentric Datum of Australia (1998) Technical manual. *Intergovernmental Committee on Surveying and Mapping (ICSM) and Permanent Committee on Geodesy (PCG)*. Canberra: Commonwealth of Australia.

Gillespie R (1977) Sydney University natural radiocarbon measurements IV. *Radiocarbon* 19: 101–110.

Gillespie R and Polach HA (1979) The suitability of marine shells for radiocarbon dating of Australian prehistory. In: Berger R and Suess H (eds) *Proceedings of the Ninth International Conference on Radiocarbon Dating*. Los Angeles, CA: University of California Press, pp. 404–421.

Grimes KG (1979) *Mornington – Cape Van Diemen, Queensland: Sheet SE/54–1/2 International Index*. Canberra: Australian Government Publishing Service.

Grindrod J and Rhodes EG (1984) Holocene sea-level history of a tropical estuary: Missionary Bay, north Queensland. In: Thom BG (ed.) *Coastal Geomorphology in Australia*. Sydney: Academic Press, pp. 151–178.

Grindrod J, Moss PT and van der Kaars S (1999) Late Quaternary cycles of mangrove development and decline on the north Australian continental shelf. *Journal of Quaternary Science* 14: 465–470.

Grindrod J, Moss PT and van der Kaars S (2002) Late Quaternary mangrove pollen records from the continental shelf and deep ocean cores in the north Australian region. In: Kershaw AP, David B, Tapper T et al. (eds) *Bridging Wallace's Lines – The Environmental and Cultural History and Dynamics of the Se-Asian-Australian Region* (Advances in Geoecology 34). Reiskirchen: Cantena Verlag, pp. 119–148.

Harris PT, Heap AD, Marshall JF et al. (2007) *Submerged coral reefs and benthic habitats of the southern Gulf of Carpentaria*. Geoscience Australia Record, 2007/02. Canberra: Geoscience Australia, 134 pp.

Harris PT, Heap AD, Marshall JF et al. (2008) A new coral reef province in the Gulf of Carpentaria, Australia: Colonisation, growth and submergence during the early Holocene. *Marine Geology* 251: 85–97.

Hearty PJ, Hollin JT, Conrad Neumann A et al. (2007) Global sea-level fluctuations during the Last Interglaciation (MIS 5e). *Quaternary Science Reviews* 26(17–18): 2090–2112.

Hendry M and Digerfeldt G (1989) Palaeogeography and palaeoenvironments of a tropical coastal wetland and offshore shelf during Holocene submergence, Jamaica. *Palaeogeography, Palaeoclimatology, Palaeoecology* 73(1–2): 1–10.

Hodgson GM (1998) Corals. In: Carpenter KE and Niem VH (eds) *The Living Marine Resources of the Western Central Pacific. Volume 1. Seaweeds, Corals, Bivalves and Gastropods* (FAO species identification guide for fishery purposes). Rome, FAO, pp. 1–686.

Hogg AG, Hua Q, Blackwell PG et al. (2013) SHCal13 Southern Hemisphere calibration, 0–50,000 cal yr BP. *Radiocarbon* 55: 1889–1903.

Hopley D (1986) Beach-rock as a sea-level indicator. In: Van de Plassche O (ed.) *Sea-Level Research: A Manual for the Collection and Evaluation of Data*. Norwich: Geo Books, pp. 157–173.

Hopley D, Smithers SG and Parnell K (2007) *Geomorphology of the Great Barrier Reef: Development, Diversity and Change*. Cambridge: Cambridge University Press, 546 pp.

Hua Q, Barbetti M, Levchenko VA et al. (2012) Monsoonal influence on Southern Hemisphere $^{14}CO_2$. *Geophysical Research Letters* 39: L19806.

Hua Q, Jacobsen GE, Zoppi U et al. (2001) Progress in radiocarbon target preparation at the ANTARES AMS Centre. *Radiocarbon* 43: 275–282.

Jones BG, Young RW and Eliot IG (1979) Stratigraphy and chronology of receding barrier beach deposits on the northern Illawarra coast of New South Wales. *Journal of the Geological Society of Australia* 26: 255–264.

Jones MR and Torgersen T (1988) Late Quaternary evolution of Lake Carpentaria on the Australian-New Guinea continental shelf. *Australian Journal of Earth Sciences* 35: 313–324.

Kershaw S and Guo L (2001) Marine notches in coastal cliffs: Indicators of relative sea-level change, Perachora Peninsula, central Greece. *Marine Geology* 179: 213–228.

Komar PD (1998) *Beach Processes and Sedimentation*. 2nd Edition. Upper Saddle River, NJ: Prentice Hall.

Lane TI, Nanson RA, Vakarelov BK et al. (2017) Evolution and architectural styles of a forced-regressive Holocene delta and megafan, Mitchell River, Gulf of Carpentaria, Australia. *Geological Society of London* 444(1): 305–334.

Lees BG (1987) Age structure of the Point Stuart chenier plain: A reassessment. *Search* 18: 257–259.

Lees BG, Lu Y and Head J (1990) Reconnaissance thermoluminescence dating of northern Australian coastal dunefields. *Quaternary Research* 34: 169–185.

Leonard ND, Welsh KJ, Zhao J-X et al. (2013) Mid-Holocene sea level and coral reef demise: U-Th dating of subfossil corals in Moreton Bay, Australia. *The Holocene* 23(12): 1841–1852.

Lewis SE, Sloss CR, Murray-Wallace CV et al. (2013) Post-glacial sea-level changes around the Australian margin: A review. *Quaternary Science Reviews* 74: 115–138.

Lewis SE, Wüst RAJ, Webster JM et al. (2008) Mid-late Holocene sea level variability in eastern Australia. *Terra Nova* 20: 74–81.

Lewis SE, Wüst RAJ, Webster JM et al. (2015) Rapid relative sea-level fall along north-eastern Australia between 1200 and 800 cal. yr BP: An appraisal of the oyster evidence. *Marine Geology* 370: 20–30.

McBride RA, Taylor MT and Byrnes MR (2007) Coastal morphodynamics and chenier-plain evolution in southwestern Louisiana, USA: A geomorphic model. *Geomorphology* 88: 367–422.

McGowan SA and Baker RGV (2014) How past sea-level changes can inform future planning: A case study from the Macleay River estuary, New South Wales, Australia. *Holocene* 24: 1591–1601.

McLean RF (2011). *Encyclopaedia of Modern Coral Reefs* (ed D Hopley). Amsterdam: Springer, pp. 107–111.

Memmott P, Round E, Rosendahl D et al. (2016) Fission, fusion and syncretism: Linguistic and environmental changes amongst the Tangkic people of the southern Gulf of Carpentaria, northern Australia. In: Verstraete J-C and Hafner D (eds) *Land and Language in Cape York Peninsula and the Gulf Country* (Culture and Language Use 18). Amsterdam: John Benjamins, pp. 105–136.

Moss PT, Mackenzie L, Ulm S et al. (2015) Environmental context for late Holocene human occupation of the South Wellesley Archipelago, Gulf of Carpentaria, Northern Australia. *Quaternary International* 385: 136–144.

Moy CM, Seltzer GO, Rodbell DT et al. (2002) Variability of El Niño/Southern Oscillation activity at millennial timescales during the Holocene epoch. *Nature* 420(6912): 162–165.

Nanson RA, Vakarelov BK, Ainsworth RB et al. (2013) Evolution of a Holocene, mixed-process, forced regressive shoreline: The Mitchell River delta, Queensland, Australia. *Marine Geology* 339: 22–43.

Neumann AC and Hearty PJ (1996) Rapid sea-level changes at the close of the Last Interglacial (Stage 5e) recorded in Bahamian Island geology. *Geology* 24: 775–778.

Nott J (1996) Late Pleistocene and Holocene sea-level highstands in Northern Australia. *Journal of Coastal Research* 12: 907–910.

Nott J, Goff J, Change-Goff C et al. (2013) Anatomy of sand beach ridges: Evidence from severe Tropical Cyclone Yasi and its predecessors, northeast Queensland, Australia. *Journal of Geophysical Research: Earth Surface* 118: 1–10.

Otvos EG (2000) Beach ridges – Definitions and significance. *Geomorphology* 32: 83–108.

Otvos EG (2004) Holocene Gulf levels: Recognition issues and an updated sea-level curve. *Journal of Coastal Research* 20(3): 680–699.

Otvos EG (2005) Validity of sea-level indicators: A comment on A new depositional model for the buried 4000 yr BP New Orleans barrier: Implications for sea-level fluctuations and onshore transport from a nearshore shelf source by F.W. Stapor and G.W. Stone [Marine Geology 204 (2004) 215–234]680–699. *Marine Geology* 217: 177–187.

Parkinson RW (1989) Decelerating Holocene sea-level rise and its influence on Southwest Florida coastal evolution: A transgressive/regressive stratigraphy. *Journal of Sedimentary Petrology* 59(6): 960–972.

Pirazzoli PA (1986) Marine notches. In: van de Plassche O (ed.) *Sea-Level Research: A Manual for the Collection and Evaluation of Data*. Norwich: Geo Books, pp. 361–400.

Pirazzoli PA (1996) *Sea-Level Changes: The Last 20,000 Years*. West Sussex: John Wiley & Sons.

Reeves JM, Barrows TT, Cohen TJ et al. (2013) Climate variability over the last 35,000 years recorded in marine and terrestrial archives in the Australian region: An OZ-INTIMATE compilation. *Quaternary Science Reviews* 74: 21–34.

Reeves JM, Chivas AR, Garcia A et al. (2007) Palaeoenvironmental change in the Gulf of Carpentaria (Australia) since the last interglacial based on Ostracoda. *Palaeogeography, Palaeoclimatology, Palaeoecology* 246: 163–187.

Reeves JM, Chivas AR, Garcia A et al. (2008) The sedimentary record of palaeoenvironments and sea-level change in the Gulf of Carpentaria, Australia, through the last glacial cycle. *Quaternary International* 183: 3–22.

Reimer PJ, Bard E, Bayliss A et al. (2013) IntCal13 and Marine13 radiocarbon age calibration curves 0-50,000 years cal BP. *Radiocarbon* 55: 1869–1887.

Rhodes EG (1982) Depositional model for a chenier plain, Gulf of Carpentaria, Australia. *Sedimentology* 29: 201–221.

Rhodes EG, Polach HA, Thom BG et al. (1980) Age structure of Holocene coastal sediments: Gulf of Carpentaria, Australia. *Radiocarbon* 22: 718–727.

Rodriguez AB and Meyer CT (2006) Sea-level variation during the Holocene deduced from the morphologic and stratigraphic evolution of Morgan Peninsula, Alabama, USA. *Journal of Sedimentary Research* 76: 257–269.

Rosendahl D (2012) *The Way it Changes like the Shoreline and the Sea: The Archaeology of the Sandalwood River, Mornington Island, Southeast Gulf of Carpetaria Australia*. Unpublished PhD thesis. Brisbane: School of Architecture, University of Queensland.

Rosendahl DE, Ulm S, Sloss CR et al. (2015) Mid-Holocene Aboriginal occupation of offshore islands in Northern Australia? A reassessment of Wurdukanhan, Mornington Island, Southern Gulf of Carpentaria, Australia. *Quaternary International* 385: 145–153.

Rovere A, Stocchi P and Vacchi M (2016) Eustatic and relative sea level changes. *Current Climate Change Reports* 2(4): 221–231.

Saito Y, Wei H, Zhou Y et al. (2000) Delta progradation and chenier formation in the Huanghe (Yellow River) delta, China. *Journal of Asian Earth Sciences* 18: 489–497.

Saito Y, Yang ZS and Hori K (2001) The Huanghe (Yellow River) and Changjiang (Yangtze River) deltas: A review on their characteristics, evolution and sediment discharge during the Holocene. *Geomorphology* 41: 219–231.

Scheffers A, Engel M, Scheffers S et al. (2011) Beach ridge systems – Archives for Holocene coastal events? *Progress in Physical Geography* 36: 5–37.

Scholl DW (1964) Recent sedimentary record in mangrove swamps and rise in sea level over the southwestern coast of Florida: Part 1. *Marine Geology* 1: 344–366.

Scholl DW, Craighead FC Jr and Stuiver M (1969) Florida submergence curve revised: Its relation to coastal sedimentation rates. *Science* 163: 562–564.

Shennan I and Horton B (2002) Holocene land- and sea-level changes in Great Britain. *Journal of Quaternary Science* 17: 511–526.

Shulmeister J (1999) Australasian evidence for mid-Holocene climate change implies precessional control of Walker Circulation in the Pacific. *Quaternary International*: 57–58: 81–91.

Shulmeister J and Lees BG (1992) Morphology and chronostratigraphy of a coastal dunefield; Groote Eylandt, northern Australia. *Geomorphology* 5(6): 521–534.

Sloss CR, Jones BG, Brooke BP et al. (2011) Contrasting sedimentation rates in Lake Illawarra and St Georges Basin, two large barrier estuaries on the southeast coast of Australia. *Journal of Paleolimnology* 46: 561–577.

Sloss CR, Jones BG, Murray-Wallace CV et al. (2005) Holocene sea level fluctuations and the sedimentary evolution of a barrier estuary: Lake Illawarra, New South Wales, Australia. *Journal of Coastal Research* 21(5): 943–959.

Sloss CR, Murray-Wallace CV and Jones BG (2007) Holocene sea-level change on the southeast coast of Australia: A review. *The Holocene* 17: 999–1014.

Sloss CR, Westerway K, Hau Q et al. (2013) Chapter: 14.36 An introduction to dating techniques: A guide for Geomorphologists. In: Shroder JF (ed.) *Treatise on Geomorphology, Vol. 14: Methods in Geomorphology*. San Diego, CA: Academic Press, pp. 119–137.

Smart J, Grimes K, Doutch H et al. (1980) *The Mesozoic Carpentaria Basin and the Cainozoic Karumba Basin, North Queensland*. Canberra: Australian Government Publishing Service.

Smithers S (2011) Sea-level indicators. In: Hopley D (ed.) *Encyclopaedia of Modern Coral Reefs: Structure, Form and Process. Encyclopedia of Earth Science*. Dordrecht: Springer, pp. 978–991.

Stattegger K, Tjallingii R, Saito Y et al. (2013) Mid to Late Holocene sea-level reconstruction of Southeast Vietnam using beach-rock and beach-ridge deposits. *Global and Planetary Change* 110(B): 214–222.

Stuiver M, Reimer PJ and Braziunas TF (1998) High-precision radiocarbon age calibration for terrestrial and marine samples. *Radiocarbon* 40: 1127–1151.

Stuiver M, Reimer PJ, Bard E et al. (1998) INTCAL98 Radiocarbon age calibration, 24,000-0 cal BP. *Radiocarbon* 40: 1041–1083.

Tamur Y (2012) Beach ridges and prograded beach deposits as palaeoenvironment records. *Earth-Science Reviews* 114: 279–297.

Tanner WF (1988) Beach-ridge data and sea-level history from the Americas. *Journal of Coastal Research* 4(1): 81–91.

Taylor MJ and Stone GW (1996) Beach-ridges: A review. *Journal of Coastal Research* 12: 612–621.

Thom BG and Roy P (1983) Sea level change in New South Wales over the past 15000 years. In: Hopley D (ed.) *Australian Sea Levels in the Last 15000 Years: A Review. Monograph Series Occasional Paper 3*. Townsville: Geography Department, James Cook University, pp. 64–84.

Thom BG and Roy P (1985) Relative sea levels and coastal sedimentation in southeast Australia in the Holocene. *Journal of Sedimentary Petrology* 55: 257–264.

Torgersen T, Hutchinson MF, Searle DE et al. (1983) General bathymetry of the Gulf of Carpentaria and the Quaternary physiography of Lake Carpentaria. *Palaeogeography, Palaeoclimatology, Palaeoecology* 41(3-4): 207–225.

Torgersen T, Luly J, De Deckker P et al. (1988) Late Quaternary environments of the Carpentaria Basin, Australia. *Palaeogeography, Palaeoclimatology, Palaeoecology* 67(3-4): 245–261.

Twaddle RW, Sloss CR, Lowe KM et al. (2017) Short-term late Holocene dry season occupation and sandy-mud flat focused foraging at Murdumurdu, Bentinck Island, Gulf of Carpentaria. *Queensland Archaeological Research* 20: 9–46.

Ulm S (2006) Australian marine reservoir effects: A guide to ΔR values. *Australian Archaeology* 63: 57–60.

Ulm S, Evans N, Rosendahl D et al. (2010) Radiocarbon and linguistic dates for occupation of the south Wellesley Islands, northern Australia. *Archaeology in Oceania* 45(1): 39–43.

Umitsu M, Buman M, Kawase K et al. (2001) Holocene palaeoecology and formation of the Shoalhaven River deltaic-estuarine plains, southeast Australia. *The Holocene* 11: 407–418.

Vousdoukas MI, Velegrakis AF and Plotmaritis TA (2007) Beachrock occurrence, characteristics, formation mechanisms and impacts. *Earth-Science Reviews* 85: 23–46.

Wang H and van Strydonck M (1997) Chronology of Holocene cheniers and oyster reefs on the coast of Bohai Bay, China. *Quaternary Research* 47: 192–205.

Weill P, Tessier B, Mouazé D et al. (2012) Shelly cheniers on a modern macrotidal flat (Mont-Saint-Michel bay, France) – Internal architecture revealed by ground-penetrating radar. *Sedimentary Geology* 279: 173–186.

Williams AN, Ulm S, Sapienza T et al. (2018) Sea-level change and demography during the last glacial termination and early Holocene across the Australian continent. *Quaternary Science Reviews* 182: 144–154.

Wolanski E (1993) Water circulation in the Gulf of Carpentaria. *Journal of Marine Systems*: 4: 401–420.

Woodroffe CD (1981) Mangrove swamp stratigraphy and Holocene transgression, Grand Cayman Island, West Indies. *Marine Geology* 41: 271–294.

Woodroffe CD (1988) Mangroves and sedimentation in reef environments: Indicators of past sea-level changes, and present sea-level trends? In: *Proceedings of the Sixth International Coral Reef Symposium*, vol. 3, Townsville, Australia, 8–12 August, pp. 535–539.

Woodroffe CD and Chappell J (1993) Holocene emergence and evolution of the McArthur River Delta, southwestern Gulf of Carpentaria, Australia. *Sedimentary Geology* 83: 303–317.

Woodroffe CD, Samosorn B, Hua Q et al. (2007) Incremental accretion of a sandy reef island over the past 3000 years indicated by component-specific radiocarbon dating. *Geophysics Research Letters* 34: L03602.

Yokoyama Y, Esat TM and Lambeck K (2001a) Last glacial sea-level change deduced from uplifted coral terraces of Huon Peninsula, Papua New Guinea. *Quaternary International* 83–85: 275–283.

Yokoyama Y, Lambeck L, De Deckker P et al. (2000) Timing of the Last Glacial Maximum from observed sea-level minima. *Nature* 406: 713–716.

Yokoyama Y, Purcell A, Lambeck K et al. (2001b) Shore-line reconstruction around Australia during the Last Glacial Maximum and Late Glacial Stage. *Quaternary International* 83–85: 9–18.

Zhou H, Zhao J, Qing W et al. (2011) Speleothem-derived Asian summer monsoon variations in Central China, 54–46 ka. *Journal of Quaternary Science* 26(8): 781–790.